

1   **First tephrostratigraphic results of the DEEP site record**  
2   **from Lake Ohrid (Macedonia, Albania)**

3   **N. Leicher<sup>1</sup>, G. Zanchetta<sup>2</sup>, R. Sulpizio<sup>3,4</sup>, B. Giaccio<sup>5</sup>, B. Wagner<sup>1</sup>, S. Nomade<sup>6</sup>,**  
4   **A. Francke<sup>1</sup>, and P. Del Carlo<sup>7</sup>**

5   [1] Institute of Geology and Mineralogy, University of Cologne, Zuelpicher Str. 49a, 50674  
6   Cologne, Germany

7   [2] Dipartimento di Scienze della Terra, University of Pisa, via S. Maria 53, 56126 Pisa, Italy

8   [3] Dipartimento di Scienze della Terra e Geoambientali, University of Bari, via Orabona 4,  
9   70125 Bari, Italy

10   [4] Istituto per la Dinamica dei Processi Ambientali (IDPA) CNR, via M. Bianco 9, Milan, Italy

11   [5] Istituto di Geologia Ambientale e Geoingegneria, CNR, Via Salaria Km 29,300,  
12   Monterotondo, Roma, Italy

13   [6] Laboratoire des sciences du climat et de l'environnement, UMR 8212, CEA/CNRS/UVSQ  
14   et Université Paris-Saclay F-91198 Gif-Sur-Yvette, France

15   [7] Istituto Nazionale di Geofisica e Vulcanologia, Sezione di Pisa, via della Faggiola 32,  
16   56126, Pisa, Italy

17

18   Correspondence to: N. Leicher (n.leicher@uni-koeln.de)

19

20

21

22

23

24

25

26

1   **Abstract**

2   A tephrostratigraphic record covering the Marine Isotope Stages (MIS) 1–15 was established  
3   for the DEEP site record of Lake Ohrid (Macedonia/Albania). Major element analyses (SEM-  
4   EDS/WDS) were carried out on juvenile fragments extracted from 12 tephra layers (OH-DP-  
5   0115 to OH-DP-2060). The geochemical analyses of the glass shards of all of these layers  
6   suggest an origin from the Italian volcanic provinces. They include: the Y-3 (OH-DP-0115,  
7   26.68–29.42 ka cal BP), the Campanian Ignimbrite/Y-5 (OH-DP-0169,  $39.6\pm0.1$  ka), and the  
8   X-6 (OH-DP-0404,  $109\pm2$  ka) from the Campanian volcanoes, the P-11 of the Pantelleria Island  
9   (OH-DP-0499,  $133.5\pm2$  ka), the Vico B (OH-DP-0617,  $162\pm6$  ka) from the Vico volcano, the  
10   Pozzolane Rosse (OH-DP- 1817,  $457\pm2$  ka), and the Tufo di Bagni Albule (OH-DP-2060,  
11    $527\pm2$  ka) from the Colli Albani volcanic district, and the Fall A (OH-DP-2010,  $496\pm3$  ka)  
12   from the Sabatini volcanic field. Furthermore, a comparison of the Ohrid record with  
13   tephrostratigraphic records of mid-distal archives related to the Mediterranean area allowed the  
14   recognition of the equivalents of other less known tephra layers, such as the TM24a/POP2 (OH-  
15   DP-0404,  $102\pm2$  ka) recognised in the Lago Grande di Monticchio and the Sulmona basin, the  
16   CF-V5/PRAD3225 (OH-DP-0624, ca.  $163\pm22$  ka) identified in the Campo Felice  
17   basin/Adriatic Sea, the SC5 (OH-DP-1955,  $493.1\pm10.9$  ka) recognised in the Mercure basin,  
18   and the A11/12 (OH-DP-2017,  $511\pm6$  ka) sampled at the Acerno basin, whose specific volcanic  
19   sources are still poorly constrained. Additionally, one cryptotephra (OH-DP-0027) was  
20   identified by correlation of the potassium XRF intensities from the DEEP site with those from  
21   a short core of a previous study from Lake Ohrid. In these cores, a maximum in potassium is  
22   caused by glass shards, which were correlated with the Mercato tephra (8.43– 8.63 ka cal BP)  
23   from Somma-Vesuvius. The presented tephrostratigraphic work allows, for the first time, the  
24   extension of a consistent part of the Middle Pleistocene tephrostratigraphy of Italian volcanoes  
25   as far as to the Balkans. The establishment of the tephrostratigraphic framework for the Lake  
26   Ohrid record provides important, independent tie-points for the age-depth model of the DEEP  
27   site sequence, which is a prerequisite for paleoclimatic and -environmental reconstructions.  
28   Furthermore, this age-depth model will help to improve and re-evaluate the chronology of other,  
29   both undated and dated tephra layers from other records. Thus, the Lake Ohrid record is  
30   candidate to become the template for the central Mediterranean tephrostratigraphy, especially  
31   for the hitherto poorly known and explored lower Middle Pleistocene period.

1    **1 Introduction**

2    Volcanic explosive eruptions produce pyroclastic material, called tephra (gr.  $\tau\epsilon\phi\rho\alpha$  = ash), which  
3    is ejected into the atmosphere and distributed by the prevailing wind systems. Tephra settles  
4    down from the atmosphere in a relatively short time (days-weeks) as isochronous event marker  
5    horizons into all kind of geological archives downwind of the volcano. By determining the  
6    unique geochemical and physical fingerprint of such a tephra horizon, tephra layers (from  
7    different archives) can be identified, characterised, and correlated with each other in order to  
8    obtain a tephrostratigraphic framework. If tephra horizons can be dated directly (e.g.,  $^{40}\text{Ar}/^{39}\text{Ar}$ )  
9    or indirectly (e.g.,  $^{14}\text{C}$  dating on overlying or underlying sediments, varve counting, age  
10   modelling) and correlated with tephra horizons in other archives, also the ages can be  
11   transferred to these other archives.

12   The Italian volcanism was characterized by an intense explosive activity during the entire  
13   Quaternary (Peccerillo, 2005). Consequently, the surrounding Mediterranean region became an  
14   ideal setting for tephrochronological studies (tephrostratigraphy and tephrochronometry, cf.  
15   Sarna-Wojcicki, 2013), which provide a key tool for a wide spectrum of Quaternary science  
16   subjects (e.g. Lowe, 2011). After Keller et al. (1978) set up the first tephrostratigraphic scheme  
17   for the central Mediterranean region, numerous studies on marine and terrestrial archives have  
18   spatially and temporally extended and improved this initial stratigraphy for the Holocene and  
19   Late Pleistocene (Paterne et al., 1986, 1988, 2008; Vezzoli, 1991; Calanchi et al., 1998; Narcisi  
20   and Vezzoli, 1999; Siani et al., 2004; Calanchi and Dinelli, 2008; Zanchetta et al., 2011;  
21   Tamburrino et al., 2012; Insinga et al., 2014; Satow et al., 2015; Tomlinson et al., 2015).  
22   Despite this noticeable progress over the last decades, tephrochronological work in the period  
23    $> 200$  ka is still challenging due to incomplete knowledge on the eruption history and limited  
24   geochemical analysis. Some records from the Italian Peninsula cover specific intervals of the  
25   Early to Middle Pleistocene and can be used as proximal (Karner et al., 2001; Rouchon et al.,  
26   2008; Marra et al., 2009, 2014; Palladino et al., 2010; Giaccio et al., 2013a) or relatively distal  
27   (Karner et al., 1999; Munno and Petrosino, 2007; Roulleau et al., 2009; Russo Ermolli et al.,  
28   2010; Giaccio et al., 2013b, 2014, 2015; Petrosino et al., 2014a, b, 2015; Sagnotti et al., 2014)  
29   archives of deposits from volcanic complexes. Sediment records spanning continuously  $> 200$   
30   ka are extremely rare in the Mediterranean region. To date, there are only two continuous  
31   records covering the entire Middle and parts of the Early Pleistocene of the Mediterranean  
32   region, which are the Calabrian Ridge core KC01B (Lourens, 2004; Insinga et al., 2014) and

1 the peat record from Tenaghi Philippon, Greece (Tzedakis, 1993; St. Seymour et al., 2004;  
2 Pross et al., 2007). However, both records are limited in the tephrostratigraphy to the Holocene  
3 and upper Middle Pleistocene.

4 Lake Ohrid is located on the Balkan Peninsula and is one of the oldest lakes of Europe (Wagner  
5 et al., 2014). Over 1.2 Ma of continuous sediments were recovered from Lake Ohrid during the  
6 ICDP (International Continental Scientific Drilling Program) deep drilling campaign  
7 SCOPSCO (Scientific Collaboration on Past Speciation Conditions in Lake Ohrid). Previous  
8 tephrochronological studies on sediment cores from Lake Ohrid covered the last 135 ka and  
9 revealed the lake's unique potential as distal tephra archive of Italian volcanoes (e.g. Sulpizio  
10 et al., 2010).

11 Here, we present first tephrostratigraphic and tephrochronological results of the uppermost  
12 247.8 m composite depth (mcd) of the main drill site (DEEP site) in the central part of the lake,  
13 which covers continuously the last 637 ka (Francke et al., 2015). The correlation of the  
14 discovered tephra layers to known and dated equivalent tephra horizons from proximal and  
15 distal archives enables dating of the Lake Ohrid succession. The transfer of these ages to the  
16 Lake Ohrid record provides important, independent tie-points for an age-depth model  
17 complemented by orbital tuning (Francke et al., 2015), which is a precondition for  
18 environmental and climate reconstructions. The correlation of tephra layers between different  
19 geographical archives, both terrestrial and marine, is crucial for a synchronisation of  
20 paleoclimatic and paleoenvironmental changes on a regional and global scale.

## 21 **2 Regional setting**

22 Lake Ohrid ( $40^{\circ}54'$ – $41^{\circ}10'$  N,  $20^{\circ}38'$ – $20^{\circ}48'$  E) is located in the Balkan Peninsula (cf. Fig.  
23 1a) and shared between Albania and the Former Yugoslav Republic of Macedonia (FYROM).  
24 The lake is 30 km long, 15 km wide, covers an area of  $358 \text{ km}^2$ , and is situated at an altitude of  
25 693 m above sea level (a.s.l.). The lake basin has a simple tub-like shape with a volume of  
26  $55.4 \text{ km}^3$  and a maximum water depth of 293 m (Lindhorst et al., 2015). The lake is oligotrophic  
27 today due to the large water volume and the low nutrient availability (Wagner et al., 2010), and  
28 has a specific conductivity of ca.  $200 \mu\text{Scm}^{-1}$  and a pH of around 8.4 (Matter et al., 2010) in  
29 the surface waters. The hydrological characteristics are mainly controlled by a relatively low  
30 water input of  $37.9 \text{ m}^3\text{s}^{-1}$ , of which ~50% derives from karst aquifers (Matzinger et al., 2006a,  
31 b). The natural catchment area is relatively small with  $1042 \text{ km}^2$  (Matzinger et al., 2006b;  
32 Wagner et al., 2008). Lake Ohrid is situated within the Lake Ohrid Basin, which is a 40 km

1 long N–S trending graben structure in the Dinarides-Albanides-Hellenides mountain belt. The  
2 basin formation was initiated during a late phase of Alpine orogeny in the Miocene as a pull-  
3 apart basin in a short transtensional phase and consequently widened by an E-W extensional  
4 phase since the Pliocene (Lindhorst et al., 2015). The exact age of the formation of the lake is  
5 still unknown and subject of several studies within the SCOPSCO project.

6 In the N and NE of the basin Palaeozoic metamorphic rocks crop out, which are superimposed  
7 by Triassic to Early Jurassic karstified platform carbonates (cf. Fig. 1b) in the E, NW and at the  
8 up to 2300 m a.s.l. high Galičica Mountains in the SE (Robertson and Shallo, 2000). Jurassic  
9 ophiolites and Tertian conglomerates form the Mocra Mountains of the SW part of the graben  
10 shoulder (Robertson and Shallo, 2000). Mesozoic intrusions of rhyolites and diabases are  
11 locally preserved in between the limestones and dolomites in the NE (Hoffmann et al., 2010).  
12 The plains in the N and S of Lake Ohrid are covered with lacustrine and alluvial plain sediments  
13 of Quaternary age (Watzin et al., 2002). The occurrence of a hydrothermal field near Kosel in  
14 the north of the Lake Ohrid Basin is most likely fault related since no hints for volcanic activity  
15 in younger times have been found during detailed field mapping (Reicherter et al., 2011).

### 16 **3 Materials and methods**

17 During the ICDP deep drilling campaign at Lake Ohrid in spring 2013 six parallel holes were  
18 drilled at the main drill site, the DEEP site (cf. Fig. 1b), down to a maximum sediment depth of  
19 569 m below lake floor (b.l.f.). The coring location (40 m distance between the individual holes)  
20 can be averaged to 41°02'57" N and 20°42'54" E with a water depth of 243 m.

21 The cores of the DEEP site sequence were opened lengthwise, visually described, and  
22 subsequently scanned by X-ray fluorescence with an ITRAX core scanner (Cr- tube, 30mA  
23 30 kV, COX Ltd, Sweden) at the University of Cologne. Based on the core description and the  
24 XRF data the uppermost 247.8 mcd of the DEEP site sequence were correlated to a composite  
25 profile (Francke et al., 2015). The core halves were visually screened for conspicuous horizons  
26 showing changes in macroscopic grain size or colour to identify potential tephra layers. Smear  
27 slides of these horizons were then checked for the occurrence of glass shards and micro-pumices  
28 using a Leitz DM EP polarization microscope. Once a tephra layer was identified, bulk samples  
29 were taken from the respective horizon and embedded in epoxy resin. The epoxy pucks were  
30 polished to avoid compositional variations due to topographic effects and carbon-coated to  
31 enable conductivity during the following SEM and EDS/WDS-analysis. A first screening of  
32 major element compositions of single glass shards and micro-pumice was done using a SEM

1 Philips XL30 equipped with an energy dispersive spectroscope (EDS) EDAX DX4. Operating  
2 conditions were adjusted at 20 kV accelerating energy, 200–500 nm beam diameter, 9–10 Å  
3 beam current, 100 s live time with 2100–2400 shots per second, and ZAF correction (Z: atomic  
4 number; A: absorption; and F: fluorescence). The initial calibration, using four reference  
5 standards (albite, olivine and the glasses CFA47 and KE12), and the performance of the  
6 machine are described in detail by Marianelli and Sbrana (1998). In order to obtain more  
7 accurate quantitative analysis and to enlarge the comparability/reproducibility with existing  
8 datasets, a second screening of the samples was performed using the more common wavelength  
9 dispersive spectrometer (WDS) technique at the Istituto di Geologia Ambientale e  
10 Geoingegneria of the Italian National Research Council (IGAG-CNR, Rome). A Cameca SX50  
11 electron microprobe equipped with a five wavelength dispersive spectrometer was set to the  
12 following operating conditions: 15 kV; beam current, 15 nA; beam diameter, 10–15 mm; and  
13 counting time 20 s per element. Wollastonite (Si and Ca), corundum (Al), diopside (Mg),  
14 andradite (Fe), rutile (Ti), orthoclase (K), jadeite (Na), phlogopite (F), potassium chloride (Cl),  
15 baritina (S), and metals (Mn) were used as standards. Titanium contents were corrected for the  
16 overlap of the Ti and K peaks. Two international secondary standards (Kanui augite and rhyolite  
17 RLS132 glasses, from the United States Geological Survey) were analysed prior sample  
18 measurements to evaluate the accuracy of the analyses. The mean analytical precision was < 1%  
19 for SiO<sub>2</sub> and up to 1, 5, 15, 30, and > 50% for all the elements in concentration range of 15-30,  
20 5-15, 1-5, 1-0.3, and < 0.3 wt %, respectively. All geochemical compositions were recalculated  
21 as being 100% water-free. The geochemically classification of the composition of shards and  
22 micro-pumice was done with the total alkali vs. silica (TAS) diagram (Le Bas et al., 1986).  
23 Identified tephra layers are labelled unambiguously with the site name (OH-DP for Ohrid-  
24 DEEP) and the correlated bottom depth of each layer (e.g. “OH-DP-corr. depth in dm”).

## 25 **4 Results and Discussion**

26 The uppermost 247.8 mcd of sediments from the DEEP site sequence mainly consist of fine-  
27 grained hemipelagic sediments with some intercalated coarse-grained beds, which were  
28 classified as event layer such as tephra and mass movement deposits. A detailed lithological  
29 description and the discussion of sedimentological processes and paleoenvironmental  
30 information is given by Francke et al. (2015). Interglacial sediments indicate high amounts of  
31 calcite and organic matter, whereas glacial sediments are dominated by clastic, terrigenous  
32 components.

1 In total, 34 macroscopic tephra layers were recognized in the upper 247.8 mcd of the DEEP site  
2 sequence (Fig. 2). 12 out of the 34 macroscopic tephra and one cryptotephra horizon have been  
3 unambiguously correlated with known eruptions of Italian volcanoes and represent the focus of  
4 the present paper. A detailed geochemical description and interpretation of the remaining tephra  
5 layers, which are not all analysed yet, and a discussion of potential ages and origins will be  
6 given elsewhere, as it is beyond the scope of this paper.

7 A local origin of the tephra layers from the direct surrounding of Lake Ohrid is highly unlikely,  
8 as there is no volcanic activity recorded for the Quaternary (cf. Fig.1). Potential volcanic  
9 sources within the Mediterranean area are the Italian provinces, the Hellenic Arc, or the  
10 Anatolian provinces. Pyroclastic deposits from the Hellenic Arc and the Anatolian provinces,  
11 mainly high-silica calc-alkaline tephra, were primarily dispersed in eastern directions (Druitt et  
12 al., 1995, 1999; Aksu et al., 2008; Hamann et al., 2010; Sulpizio et al., 2013; Sumita and  
13 Schmincke, 2013; Keller et al., 2014; Tomlinson et al., 2015), and so far have not been found  
14 in the sediment records of Lake Ohrid (Sulpizio et al., 2010) and nearby Lake Prespa  
15 (Damaschke et al., 2013). Furthermore, they were not found in the numerous studied  
16 teprochronological successions from the Tyrrhenian, Adriatic, or Western Ionian Sea.

17 Mainly eastern distribution is also assumed for Italian tephra layers, and some of them were  
18 even found in the Eastern Mediterranean and Aegean Sea (Margari et al., 2007; Sulpizio et al.,  
19 2010; Karkanas et al., 2015; Satow et al., 2015). All tephra layers discussed here show an  
20 alkaline affinity, which is only known from the Italian volcanic provinces in the Mediterranean  
21 region (Peccerillo, 2005). The existing records from lakes Ohrid and Prespa only contain tephra  
22 from Italian volcanoes, which was transported by the prevailing westerlies with E–SE directions  
23 in the upper atmospheric wind system. The Quaternary Italian volcanism is classified in several  
24 magmatic provinces (Washington, 1906; Peccerillo, 2005), which are mainly located along the  
25 Tyrrhenian coast of the Italian Peninsula, in the Tyrrhenian Sea, and in the Sicily channel,  
26 between 500 and 1000 km apart of Lake Ohrid (Fig. 1). In the studied succession (< 637 ka)  
27 explosive volcanic activity of Italian volcanoes is known so far from the Roman province  
28 (Vulsini, Vico, Sabatini, Colli Albani), the Ernici-Roccamonfina area (Mt. Ernici,  
29 Roccamonfina), the Campania province (Somma-Vesuvio, Campi Flegrei, Procida, Ischia), the  
30 Pontine Islands (Ventotene, Santo Stefano), the Mount Vulture, the Aeolian Arc (Alicudi,  
31 Filicudi, Salina, Lipari, Vulcano, Panarea, Stromboli), and the Sicily province (Mt. Etna,  
32 Ustica, Pantelleria, Fig. 1, Peccerillo, 2005). The products of these Italian volcanoes span a wide

1 compositional field ranging from subalkaline to alkaline and from mafic to silicic, depending  
2 on their geodynamic setting or mantle source (Lustrino et al., 2011). Most of them have a  
3 potassium or a high potassium affinity (Roman, Roccamonfina, Campanian, and Pontine  
4 Islands) and their large chemical similarity or overlap in composition makes tephrostratigraphic  
5 work very challenging (Sulpizio et al., 2010). An origin from one of these provinces is supposed  
6 by the (high) alkaline phonolitic and trachytic compositions of most of the tephra layers found  
7 in the DEEP site sequence. However, some of the tephra layers in the DEEP site succession  
8 show more specific and unique compositions, which allow more straightforward correlations  
9 to the Pantelleria Islands and Somma-Vesuvius (Peccerillo, 2005), or the silica undersaturated,  
10 low evolved pyroclastic products of Colli Albani (Giaccio et al., 2013a).

11

## 12 **4.1 OH-DP-0027/Mercato**

13 Cryptotephra OH-DP-0027 was recognized by correlating the patterns of the XRF potassium  
14 curve of the DEEP site record with those of the nearby core Co1262 (cf. Fig. 1, Wagner et al.,  
15 2012). In both cores, a potassium peak is observed in the same stratigraphic position, which in  
16 core Co1262 is caused by the presence of glass shards of cryptotephra Co1262-709. In the  
17 DEEP site sequence, the corresponding peak culminates at about 2.775 mcd. A microscopic  
18 inspection of the interval 2.770-2.780 mcd revealed the occurrence of glass shards. Since  
19 cryptotephra is dispersed in the sediment and do not form a continuous distinct horizons, the  
20 exact depth of the tephra isochron was set to the maximum of the K-peak (2.775 mcd), most  
21 likely representing the maximum shard concentration.

22 The discovered volcanic particles of OH-DP-0027 are highly vesicular micro-pumices having  
23 spherical or elongated vesicles and glass shards with thick septa or a platy shape. The  
24 composition of OH-DP-0027 is Na-phonolitic (Table 1, Figure 2a) and thus similar to  
25 cryptotephra Co1262-709 (Wagner et al., 2012) and the associated cryptotephra horizons  
26 OT0702-3 from Lake Ohrid (Vogel et al., 2010) and PT0915-2 from Lake Prespa (Damaschke  
27 et al., 2013). Nevertheless, OH-DP-0027 has slightly lower SiO<sub>2</sub> (2-3 wt%), and FeOTOT (~0.5  
28 wt%) contents, but higher Na<sub>2</sub>O (~1 wt%) and Al<sub>2</sub>O<sub>3</sub> (~2 wt%) contents (cf. Table 1). Despite  
29 these geochemical differences, the general geochemical signature (Na-phonolitic, cf. Suppl. I  
30 Fig. a), and the stratigraphic position of OH-DP-0027 suggest a correlation with the  
31 aforementioned cryptotephra horizons and their supposed origin, the Pomici di Mercato (PdM)

1 eruption from the Somma-Vesuvius volcano. The PdM eruption is the only known eruption in  
2 the Late Pleistocene and early Holocene having such a composition in the central Mediterranean  
3 region (Mele et al., 2010; Santacroce et al., 2008).

4 The products of the PdM eruption are found as two distinct layers TM6a and TM6b in the Lago  
5 Grande di Monticchio record (Wulf et al., 2004). The double layer were interpreted as due to  
6 shortly interrupted eruptive phases of the eruption (Mele et al., 2011). OH-DP-0027 and the  
7 associated Ohrid cryptotephra horizons match better with TM6b (Table1, cf. Suppl. I Figure a),  
8 which represents the main Plinian and initial phase of the eruption (Wulf et al., 2004). A  
9 correlation with the PdM eruption is also established for a tephra found in the Veliko Jezero on  
10 the Island of Mljet (Croatia), where even more than two eruptive phases are indicated (Jahns  
11 and van den Bogaard, 1998). Also in sediment cores from the Adriatic Sea, such as KET8218  
12 (V1, Paterne et al., 1988), IN68-9, IN68-5 and RF95-11 (125, 259, 320 cm respectively,  
13 Calanchi and Dinelli, 2008), AD91-17 (190-191, 195-196 cm, Marchini et al., 2014), or from  
14 MD90-918 (210/223cm, Caron et al., 2012) tephra layers were correlated with the PdM eruption  
15 (cf. Suppl. I Figure a).

16 Santacroce et al. (2008) reviewed several existing  $^{14}\text{C}$  ages on proximal deposits of the Mercato  
17 eruption and suggested a maximum age of 9010–8750 year cal BP. This age is somewhat  
18 younger than the varve age obtained from the Lago Grande di Monticchio record for TM6b  
19 ( $9680 \pm 480$  year BP; Wulf et al., 2004). The most reliable age of 8630-8430 year cal BP comes  
20 probably from  $^{14}\text{C}$  dating of charcoals collected at the basal part of the proximal fallout deposit  
21 (Zanchetta et al., 2011).

## 22 **4.2 OH-DP-0115 / Y-3**

23 Tephra layer OH-DP-0115 (11.492–11.507 mcd) is 1.5 cm thick, brownish-greyish in colour  
24 and has sharp upper and lower boundaries. OH-DP-0115 comprises both highly vesicular  
25 micro-pumices with elongated vesicles and bubble-wall and -junction glass shards. The glass  
26 composition is mainly trachytic tending towards the phonolitic field in the TAS-diagram (Fig.  
27 3b, Table 1), which suggests a correlation with the prominent marine tephra layer Y-3 from the  
28 Campanian area (cf. Table 1, Suppl. I Fig. b; Keller et al., 1978; Albert et al., 2015). The slightly  
29 heterogeneous major element composition, with a low and a high silica end-member (</> 62  
30 wt.%  $\text{SiO}_2$ ) is defined by Albert et al. (2015) as the diagnostic characteristic of the Y-3 tephra  
31 and perfectly matches the OH-DP-0115 tephra (cf. Fig.3b, Tab. 1, Suppl. I Fig. b). The most

probable source of the Y-3 tephra is the Campi Flegrei (CF) caldera (Di Vito et al., 2008; Zanchetta et al., 2008; Albert et al., 2015), but to date none of the suggested proximal counterparts of different eruptions could be unambiguously assigned as its origin (Albert et al., 2015). Furthermore, the former most accepted correlation of the Y-3 tephra with the intracaldera VRa and the mid-distal SMP1e/CE1 deposits (Sulpizio et al., 2003; Di Vito et al., 2008) is rejected, because new geochemical data gained on the Y-3 type locality (marine cores M25/4-12, RC9 191) separate the Y-3 from other CF eruptions of the Tufi Biancastri/NYT series (Tomlinson et al., 2012; Albert et al., 2015).

The Y-3 tephra is known as a widespread stratigraphic marker found in different archives in the Central and Eastern Mediterranean region, such as the Lago Grande di Monticchio (TM15, Wulf et al., 2004; Tomlinson et al., 2012), the Southern Adriatic Sea core MD90-917 (920/17, Zanchetta et al., 2008), Lake Ohrid (OT0520-2; OT0700-1; OT0702-4; JO 187, summarized in Sulpizio et al., 2010), Lake Prespa (PT0915-5, Damaschke et al., 2013), and the Tenaghi Philippon peat record in Greece (TP 9.70, Albert et al., 2015). These correlations are validated by the low and high silica end-member (Albert et al., 2015). The correlations of the marine tephra layers C-7 (Tyrrhenian and Adriatic Sea, Paterne et al., 1988), A2/B2 (C106/C45, Munno and Petrosino, 2004), and the terrestrial S19 layer (Munno and Petrosino, 2007) with the Y-3 tephra were not reevaluated by Albert et al. (2015) due to restricted data sets, but seem to be likely.

Since no proximal equivalents could be unambiguously identified so far, the ages from these proximal correlations (e.g., 31–30 ka cal BP, Zanchetta et al., 2008) have to be rejected (Albert et al., 2015). However, a Bayesian age-depth model based on multiple radiocarbon ages above and below the TP 9.70 tephra of the Tenaghi Phillipon record provides an age of 28.68–29.42 ka cal BP (Albert et al., 2015). This is probably the best age estimate, which is supported by radiocarbon ages from other distal archives, for example the  $^{14}\text{C}$ -age of 28.78–29.98 ka cal BP obtained at the top of the Ohrid tephra OT07042-4/Y-3 (Vogel et al., 2010). The Y-3 tephra represents an important marker in the Mediterranean area, linking marine and terrestrial archives close to the Marine Isotope Stage 3/2 transition and the North Atlantic Heinrich Stadial 3 (HS3).

30

1   **4.3 OH-DP-0169 / Y-5 CI**

2   Tephra OH-DP-0169 (16.783–16.933 mcd) has a thickness of 15 cm, which is the thickest  
3   tephra layer found within this part of the DEEP site sequence and can be visually separated into  
4   two units. The lower unit (OH-DP-0169a) has a sharp boundary at the bottom, is 2 cm thick  
5   and pale yellow in colour, whereas the upper unit (OH-DP-0169b) is 13 cm of pale brown,  
6   coarser material. The uppermost centimetres of the upper unit are mixed with lacustrine  
7   sediments and have an uneven top boundary, which is probably due to a difficult penetration  
8   during coring. Both units comprise elongated vesicle bearing micro-pumices, bubble-wall and  
9   -junction shards with thick septa, and have the same trachytic to phono-trachytic glass  
10   composition (Fig. 3c, Table 1). The characteristic trachytic to phonotracytic alkaline  
11   composition of OH-DP-0169 (cf. Fig. 3c, Suppl. I Fig. c) and its remarkable thickness allow an  
12   unambiguous correlation with the Campanian Ignimbrite (CI) eruption (Orsi et al., 1996;  
13   Civetta et al., 1997; Pappalardo et al., 2002) and the marine tephra layer Y-5 (Keller et al.,  
14   1978; Thunell et al., 1979). The comparison of major element oxides such as  $\text{Al}_2\text{O}_3$ ,  $\text{FeO}_{\text{TOT}}$ ,  
15   and  $\text{CaO}$  strongly support the correlation with the Y-5/CI deposits and exclude other possible  
16   correlation with pre-CI deposits described in Tomlinson et al., 2012 (cf. Suppl. I Fig. c).  
17   Additionally, the CI/Y-5 was also recognized in previous studies at lakes Ohrid and Prespa  
18   (OT0520-3; OT0700-2; OT0701-1; OT0702-6; JO-244; PT0704-3 summarized in Sulpizio et  
19   al., 2010).

20   The proximal deposits of the CI are described to have a trimodal composition, which resulted  
21   from the different timing and dynamic of extraction and mingling of two layered  
22   compositionally different magmas (Civetta et al., 1997; Pappalardo et al., 2002; Marianelli et  
23   al., 2006). According to Civetta et al. (1997), OH-DP-0169 belongs to the most evolved  
24   composition ( $\text{K}_2\text{O}/\text{N}_2\text{O}$  1.1–1.35) and only some shards can be assigned to the intermediate  
25   group ( $\text{K}_2\text{O}/\text{N}_2\text{O}$  1.37–1.42, cf. Suppl. II). The third, least evolved group ( $\text{K}_2\text{O}/\text{Na}_2\text{O} > 2$ ) was  
26   not found in OH-DP-0169 most likely due to its relatively low abundance in distal settings and  
27   the limited number of analysis of OH-DP-0169. Indeed, the least-evolved group is associated  
28   with the less energetic phase of the eruption of the late caldera collapse that generated more  
29   dense pyroclastic flows that did not reach great distance from the vent (Civetta et al., 1997).  
30   Thus, they are likely less representative in very distal settings also because the intermediate and  
31   most evolved group form more than 85 % of the eruptive volume (Civetta et al., 1997).

1 As the two optical units of OH-DP-0169 (a+b) cannot be geochemically discriminated based  
2 on major elements, the initial Plinian phase (cf. Marianelli et al., 2006) may correspond with  
3 the lower, pale yellow and more fine-grained part (OH-DP-0169a), while the main ignimbrite  
4 phase probably corresponds with the upper, pale brown and coarser part (OH-DP-0169b).

5 The CI/Y-5 tephra layer, originating from the Campi Flegrei (e.g. Pappalardo et al., 2002), is  
6 the most widely dispersed tephra marker in the Mediterranean region. It was found, for  
7 example, in sediment cores from the Lago Grande di Monticchio (TM-18, Wulf et al., 2004),  
8 the San Gregorio Magno basin, (S-17, Munno and Petrosino, 2007) the Greek island of Lesvos  
9 (ML 2, Margari et al., 2007), and the Tenaghi Philippon peat record (TP-CI, Lowe et al., 2012).  
10 Furthermore, it was identified in the Tyrrhenian Ses cores KET- 8022, -8004, -8003, -8011 (C-  
11 13, Paterne et al., 1988; Ton-That et al., 2001), in the Adriatic Sea cores PRAD1-2 (PRAD1653,  
12 Bourne et al., 2010) and KET8218 (C-13, Paterne et al., 1988), in the Ionian Sea cores KC01B  
13 (I-3, Insinga et al. 2014) and RC9 191/V110 69 (Y-5, Keller et al. 1978), and in the Levantine  
14 and Aegean Sea cores (RC 9 183, -181, V10 58 (Y-5) Keller et al., 1978; LC21 (4.925) Lowe  
15 et al., 2012, Satow et al., 2015). To date, the most distal finding is in the Russian Plain, 2500  
16 km away from its source (Pyle et al., 2006; Giaccio et al., 2008).

17 The ages for the CI cluster around 40 ka BP. The varve chronology of Lago Grande di  
18 Monticchio yielded an age of 36.77 ka BP (Wulf et al., 2006).  $^{40}\text{Ar}/^{39}\text{Ar}$  dating on single  
19 sanidine crystals revealed ages of  $37.1 \pm 0.4$  ka (Deino et al., 1994),  $41.1 \pm 2.1$  ka (Ton-That et al.  
20 (2001) and  $39.28 \pm 0.11$  ka (De Vivo et al., 2001), with the latter regarded as the best age, as it  
21 derives from proximal deposits.

#### 22 **4.4 OH-DP-0404 / TM24a POP2**

23 Tephra layer OH-DP-0404 (40.456–40.486 mcd) is a 3 cm thick dark reddish brown horizon  
24 with sharp stratigraphic contacts at the top and bottom. The layer comprises elongated vesicular  
25 micro-pumices and thick walled bubble-wall shards. Glass composition analyses reveal a  
26 mainly phonolitic composition with some shards scattering around the intersection of  
27 tephriphonolitic, trachyandesitic, and trachytic fields in the TAS-diagram (Fig. 3d, Table 1)  
28 The geochemical signature is similar, even if somewhat more variable, to tephra OT-0702-8  
29 (cf. Fig.3d, Suppl. I Fig. d), found in Ohrid core Co1202 (Vogel et al., 2010), which is correlated  
30 with the Monticchio tephra TM24a (Wulf et al., 2004; Wulf et al., 2012). The TM24a tephra  
31 was first correlated with the prominent marine X-5 layer (Keller et al., 1978), but this

correlation was later revised and the older Monticchio tephra TM25 was correlated with the X-5 layer (Wulf et al., 2012). The proximal or the marine tephra counterparts of TM24a remain unknown so far. Based on major element compositions, OH-DP-0404 can be further correlated with the recently found POP2 tephra in the Popoli section from the Sulmona basin (Regattieri et al., 2015), which is also correlated with the TM24a tephra (cf. Table1, Suppl. I Fig. d). A correlation of OH-DP-0404 with marine tephra layers from core CM92-42 (710 cm) and core RF93-77 (797 cm), which were also correlated with the TM24 (Calanchi and Dinelli, 2008), is likely, however, there is no differentiation between the bifurcation of tephra TM24 (a+b) in these marine tephra layers. According to the Monticchio varve record, TM24a has an age of 101.8±5 ka BP (Wulf et al., 2012), which matches well the age of 102.0±2.4 ka obtained from the age-model of the Sulmona basin (Regattieri et al., 2015).

## 4.5 OH-DP-0435 / X-6

Tephra OH-DP-0435 (43.498–43.513 mcd) is a 1.5 cm thick, greyish brown layer with sharp top and bottom contacts. The horizon comprises highly vesicular micro-pumices and bubble wall shards with thick septa having a low alkali ratio (LAR) trachytic glass composition with only few shards plotting in the phonolitic field. This geochemical composition and the position below OH-DP-0404/TM24a/POP2 suggest a correlation of OH-DP-0435 with the marine tephra layer X-6 (core 22M-60, Keller et al., 1978). The correlation is supported by the geochemically similarity of OH-DP-0435 with the Ohrid tephra layers OT0702-9 (Vogel et al., 2010) and JO-575 (Caron et al., 2010), which were also correlated with the X-6 layer (cf. Fig.3e; Suppl. I Fig. e). Equivalents of the X-6 tephra are also found in marine cores KET8004 and -8022 of the Tyrrhenian Sea (C-31, Paterne et al., 2008), the Adriatic Sea cores PRAD1-2 (PRAD-2812, Bourne et al., 2015), and the Ionian Sea cores KC01B (I-9, Insinga et al., 2014), and KET82-22 (C-31, Paterne et al., 2008). Furthermore, the X-6 is known from the terrestrial records of the Lago Grande di Monticchio (TM27, Wulf et al., 2012), the San Gregorio Magno basin (S10, Munno and Petrosino, 2007), the Cilento coastline (SM1-2/SA, Marciano et al., 2008; CIL2, Giaccio et al., 2012), and the Popoli section of the Sulmona basin (POP4, Regattieri et al., 2015). The origin of the X-6 is assigned to an unknown eruption of the Campanian area (Keller et al., 1978; Paterne et al., 2008; Wulf et al., 2012).

Based on  $^{40}\text{Ar}/^{39}\text{Ar}$  dating, the age of tephra layer X-6 is 107±2 ka (Kraml, 1997), which fits to the varve-based age of ca. 108.3±5.4 ka BP of the TM-27 layer in Lago Grande di Monticchio (Wulf et al., 2012) and the interpolated age of 107 ka of the C-31 tephra layer (Paterne et al.,

1 2008). More recently, a  $^{40}\text{Ar}/^{39}\text{Ar}$  age of  $108.9 \pm 1.8$  ka was obtained on X-6 equivalent deposits  
2 of the Cilento offshore area (t1 tephra, Iorio et al., 2014), which matches well the interpolated  
3 age of the Popoli section ( $109.0 \pm 1.5$  ka, Regattieri et al., 2015).

4

5 **4.6 OH-DP-0499 / P-11**

6 The OH-DP-0499 (49.937–49.947 mcd) tephra layer is 1 cm thick, olive brown, and  
7 characterised by a sharp bottom and a diffuse top boundary. It comprises elongated vesicular  
8 micro-pumices and larger platy bubble wall shards. OH-DP-0499 has a distinct bimodal glass  
9 chemical composition, with a clearly separated trachytic and a rhyolitic group (Fig. 3f, Table  
10 1). The shards can be classified as comendites and pantellerites (cf.  $\text{Al}_2\text{O}_3$ - $\text{FeOTOT}$  diagram,  
11 Fig.4), which unambiguously assign them to an origin from the Pantelleria Island, the only  
12 source of these type of magmas in the central Mediterranean region (Peccerillo, 2005). The  
13 twofold composition is explained by a chemically zoned magma chamber, in which peralkaline  
14 rocks originating from mantle-derived parental magma and trachytic magma differentiated in a  
15 low-pressure magma chamber by crystal-liquid fractionation (Civetta et al., 1984).

16 The stratigraphic position of OH-DP-0499, below the X-6 tephra (OH-DP-0435), infers a  
17 definite correlation with the P-11 tephra (cf. Fig. 3f) found in the Ionian Sea core KET82-22  
18 (Paterne et al., 2008), since other widespread eruptions of the Pantelleria Island are much  
19 younger (ca. 77 ka, P-10, Paterne et al., 2008; 45.7 ka, Green Tuff, Scaillet et al., 2013).  
20 Furthermore, the geochemical fingerprint of OH-DP-0499 is identical to those of the two  
21 cryptotephra layers OT0702-10 (Vogel et al., 2010) and JO-941 (Caron et al., 2010), which  
22 were found previously in Lake Ohrid sediments and correlated with the P-11 (cf. Suppl. I Fig.  
23 f). A more proximal core from the Sicily Channel (ODP 963A) comprises three pantelleritic  
24 layers (ODP2-4) in a similar stratigraphic position (Tamburrino et al., 2012). ODP2 shows a  
25 somewhat different geochemical composition (benmoritic part) compared to OH-DP-0499/P-  
26 11 (cf. Table1, Suppl. I Fig. f). ODP3 and ODP4 indicate a very similar composition, but ODP3  
27 is formed as a distinct horizon, whereas ODP4 is a cryptotephra (Tamburrino et al., 2012). Due  
28 to chronological concerns, Tamburrino et al. (2012) correlated ODP3 with the P-11, which is  
29 supported by their climastratigraphic position at the transition from MIS 6 to 5 (cf. Zanchetta  
30 et al., this issue). As only one pantelleritic layer is found in distal archives, ODP2 was precluded

1 due to chemical considerations, ODP4 is a cryptotephra, a correlation of ODP3 with the P-11  
2 layer is the most likely and supposes that this tephra is the most widespread.

3 OH-DP-0499 can be further correlated with the ML5 tephra found on Lesovs Island (Margari  
4 et al., 2007), as already suggested by Vogel et al. (2010) for the OT0702-10 tephra. The ML5  
5 tephra was previously correlated with the younger Green Tuff/Y-6, but the geochemical data  
6 support a correlation with the older P-11 tephra. In more recent studies, Karkanas et al. (2015)  
7 correlated a pantelleritic cryptotephra (THP-TII5) found in the Theopetra cave in central Greece  
8 with the P-11 and its equivalents. Satow et al. (2015) found a cryptotephra (LC21 10.345) in  
9 the Aegean Sea core LC21, which he ascribed to one of the ODP2-4 tephra layers. The position  
10 of LC21 10.345 in the *G. ruber*  $\delta^{18}\text{O}$  record of LC21 implies a correlation with ODP3 and P-  
11 based on the position in the respective isotope records. Nevertheless, it has to be stated that  
12 only the rhyolitic endmember of P-11 was found in the records from LC21 and Theopetra. The  
13 typical comenditic trachytic part is not found in these archives, which is probably due to a  
14 different dispersal of the twofold zonation of the magma chamber (rhyolitic/trachytic part)  
15 tapped at different phases of the eruption. This is also indicated by an internal zonation of the  
16 ODP3 layer. Whereas the bottom of ODP3 has a pantelleritic composition, its top shows  
17 comenditic trachytic compositions (Tamburrino et al., 2012). This suggests that the rhyolitic  
18 pantelleritic part was erupted first and dispersed over a larger area, while the comenditic  
19 trachytic part is distributed only in a smaller, northern sector. Changes of the plume direction  
20 and dispersal during an eruption are likely due to changes in the aerodynamic characteristics of  
21 the erupted material or in the high and low atmosphere dynamics (Sulpizio et al., 2008, 2013).

22 Proximal counterparts of the P-11 are the ignimbrite deposits of the P-unit on Pantelleria Island  
23 (Mahood and Hildreth, 1986; Paterne et al., 2008; Tamburrino et al., 2012). These proximal  
24 P-unit deposits provide inhomogeneous  $^{40}\text{Ar}/^{39}\text{Ar}$  ages between  $123\pm1.6$  ka and  $135\pm1.2$  ka,  
25 with large internal age variations suggesting xenocrystic contamination (Rotolo et al., 2013).  
26 The mean age of the P-unit ( $129\pm5.9$  ka) is in broad accordance with the non-radiometric ages  
27 from the distal deposits. The age-depth model of core KET82-22, based on orbital tuning of the  
28 oxygen isotope and sapropel stratigraphy, provided an age of  $130.6\pm5$  ka for the P-11 tephra  
29 (Paterne et al., 2008). This age matches well the age of 128.1 ka of ODP3, which is inferred  
30 from correlation of benthic and planktonic foraminifera  $\delta^{18}\text{O}$  curves of core ODP-963A with  
31 the SPECMAP stack curve (Incarbona et al., 2008; Tamburrino et al., 2012). The correlation of  
32 LC21 10.345 with P-11 provides an age of  $133.5\pm2$  ka, based on the correlation of the surface-

1 water foraminiferal  $\delta^{18}\text{O}$  record of LC21 to the high resolution U/Th dated Soreq Cave  $\delta^{18}\text{O}$   
2 record (Grant et al., 2012, Satow et al., 2015).

3

4 **4.7 OH-DP-0617 / Vico “Ignimbrite B”**

5 The tephra layer OH-DP-0617 (61.701–61.726 mcd) is a yellowish brown, 2.5 cm thick deposit  
6 with sharp bottom and top contacts. The very fine-grained glass shards have various forms,  
7 being highly vesicular with circular and oval bubbles. Micropumices with elongated vesicles  
8 are rare. The characteristic homogenous phonolitic composition of OH-DP-0617 (Fig. 3f, Table  
9 1) is very similar to the composition of tephra OT0701-6 (cf. Fig. 5a), which was found in the  
10 Ohrid core Co1201 (Sulpizio et al., 2010). OT0701-6 was previously correlated with the marine  
11 tephra C-20 and the proximal deposits of the SA3-b eruption from the Campanian area (Sulpizio  
12 et al., 2010). However, the stratigraphic position of OH-DP-0617 below the X-6/C-31/OH-DP-  
13 0435 and P-11/OH-DP-0499 tephra suggests that OH-DP-0617 and OT0706-1 rather  
14 correlate with the CF-V4 tephra from the Campo Felice Basin (Giraudi et al., 2011). The CF-  
15 V4 tephra is correlated with the “Ignimbrite B” of the Vico volcano (Vico B, Ronciglione  
16 Formation, Bear et al., 2009), which also has a large geochemical similarity to the Ohrid tephra  
17 layers OH-DP-0617/OT0701-6 (cf. Table 1, Fig. 5a). So far, equivalents of this Vico eruption  
18 were not found in other archives. Laurenzi and Villa (1987)  $^{40}\text{Ar}/^{39}\text{Ar}$  dated the Ignimbrite B  
19 in a proximal setting to  $157\pm3$  ka.

20

21 **4.8 OH-DP-0624 / CF-V5/ PRAD3225**

22 Tephra OH-DP-0624 (62.367–62.413 mcd) is 4.6 cm thick, of olive brown colour, and has a  
23 sharp bottom and more diffuse top transition. It comprises micro-pumices with elongated  
24 vesicles, cuspatate glass shards, and non-vesicular, blocky, porphyric particles, bearing prismatic  
25 microlites and phenocrysts. In the uppermost diffuse part, volcanic fragments are mixed with  
26 authigenic siderite crystals. The glass composition spans from the phonotephritic to the  
27 phonolitic field of the TAS-diagram (Fig. 3g, Table 1). This characteristic is also observed for  
28 tephra OT0701-7 in core Co1201 from Lake Ohrid (Sulpizio et al., 2010). OT0701-7 was first  
29 subdivided into three different chemical groups (a-b-c), of which OT0701-7b tentatively was  
30 correlated with the tephra layer OT0702-8/TM24a/X-5 (Sulpizio et al., 2010). However, this

correlation is not supported by the stratigraphic position of OT0701-7 below OT0701-6, as the latter correlates well with OH-DP-0617. Furthermore, OT0702-8/TM24a is correlated with OH-DP-0404, which is embedded by sediments of interglacial MIS5, whereas glacial sediments encompass OT0701-7 (Sulpizio et al., 2010). Also the glass composition of OT0701-7, showing a linear geochemical trend rather than two different geochemical populations, makes a correlation with OH-DP-0624 more likely (Fig. 5b).

The peculiar geochemical trend of OH-DP-0624 (cf. Fig. 3g, Fig. 5b) matches the marine tephra PRAD3225 from the Adriatic Sea (Bourne et al., 2015), which is tentatively correlated with the tephra 322 from core RF95-7 and with the TM38 tephra from the Lago Grande di Monticchio record (Wulf et al., 2012). Tephra 322 was assigned to the Vico D eruption (Calanchi and Dinelli, 2008), which is dated to ca. 138 ka (Laurenzi and Villa, 1987). TM38 has an age of  $125.6 \pm 6.3$  ka according to the varve chronology of the Lago Grande di Monticchio record (Wulf et al., 2012). However, the ages of TM38 and 322/Vico D are significantly too young for the stratigraphic position of OH-DP-0624 below the OH-DP-0617/Vico B and dated to ca.  $157 \pm 3$  ka. Another marine counterpart of OH-DP-0624 could be tephra C-42 with its phonotephritic composition (core DED8708, Paterne et al., 2008), but the published average values do not allow a robust correlation.

The most reliable equivalent of OH-DP-6024/OT0701-7/PRAD3225 is probably found in the Campo Felice basin in the Apennine chain. The geochemical composition and the stratigraphic position of the CF-V5 tephra, which was found in this basin directly below the CF-V4 tephra (Giraudi and Giaccio, 2015) correlates well with the composition and stratigraphic position of the OH-DP-6024 directly below the OH-DP-0617 tephra. Giraudi and Giaccio (2015) tentatively suggest that the CF-V5 tephra is an equivalent of the Pitigliano Tuff from the Latera caldera in the Vulsini volcanic complex (Turbeville, 1992a). Although the geochemical dataset is limited, a similar characteristic trend is observed in CF-V5 and OH-DP-0624/OT071-7/PRAD3225 (cf. Fig. 5b).  $^{40}\text{Ar}/^{39}\text{Ar}$  dating on proximal deposits of the Pitigliano Tuff provided ages of  $158 \pm 11$  ka and  $155 \pm 11$  ka (Turbeville, 1992b, a) and the overlying Vico Ignimbrite B tephra limits the minimum age to  $157 \pm 3$  ka.

29

1   **4.9 OH-DP-1817 / Pozzolane Rosse**

2   Tephra layer OH-DP-1817 (181.744–181.769 mcd) is a dark brownish layer with a thickness  
3   of 2.5 cm and sharp bottom and top contacts. The layer contains mostly non-vesicular, blocky  
4   porphyric shards with a high content of microlites and phenocrysts, mostly leucite. Vesicular  
5   cuspatate shards are rare and are also porphyritic. OH-DP-1817 has a low evolved K-foiditic  
6   composition (Fig. 3h, Table 1), which is only known from the Italian volcanoes of the Colli  
7   Albani volcanic district, and more sporadically in Vulture volcano (Peccerillo, 2005). However,  
8   as the activity of the Vulture volcano clustered between ~740 to 610 ka and around 140 ka  
9   (Villa and Buettner, 2009), the most relevant source of foiditic tephra is the Colli Albani  
10   caldera, of which the Middle Pleistocene explosive activity was characterized by very high-  
11   energetic events (e.g., Marra et al., 2009). The most widespread Colli Albani tephra is from the  
12   Pozzolane Rosse eruption (Giaccio et al., 2013a) of the Tuscalano-Aretemisio phase (~560-  
13   360 ka; Marra et al., 2011).

14   A direct chemical correlation of OH-DP-1817 with proximal Pozzolane Rosse pyroclasts is  
15   difficult, because of the lack of a comprehensive geochemical dataset. Marra et al. (2009)  
16   describe the proximal type localities (within the Colli Albani volcanic district) of the Pozzolane  
17   Rosse pyroclastic products, but only the mean value of one geochemical analysis is published  
18   (AH-20-PRa). Another, more comprehensive data set for the composition of the proximal  
19   Pozzolane Rosse pyroclastics was provided by Freda et al. (2010), who however reported only  
20   the composition of the basal sub-Plinian fallout. Therefore, the correlation OH-DP-  
21   1817/Pozzolane Rosse (cf. Fig. 3h, 5c, Suppl. I Fig. g) is mainly based on the major element  
22   data of the  $^{40}\text{Ar}/^{39}\text{Ar}$  dated distal equivalents of the Pozzolane Rosse units, which occur  
23   diffusely in the fluvial-lacustrine successions of the Apennine intermountain basins of  
24   Paganica-San Demetrio-Castelnuovo and Sulmona, east of Colli Albani (Galli et al., 2010;  
25   Giaccio et al., 2013a). Giaccio et al. (2013a) separates the Pozzolane Rosse distal equivalents  
26   into two sublayers, which differ chemically and morphologically. OH-DP-1817 matches both  
27   compositions of the less evolved composition (group a) of the lower layer and the more evolved  
28   composition (group b) of the upper sublayer (cf. Fig. 3h). Besides the geochemical correlation,  
29   microtextural features, such as the scoria character (dense, few vesicles) of the shards and the  
30   huge number of juvenile crystals, suggest the components of the lower sub-layer prevail in OH-  
31   DP-1817. Giaccio et al. (2013a) correlate the lower sublayer (group a) to the proximal  
32   Pozzolane Rosse basal fallout and the upper sublayer to the phoenix cloud of the main

1 pyroclastic flow-forming phase. According to Freda et al. (2011), the Pozzolane Rosse eruption  
2 sequence encompasses from bottom to top the Vallerano lava flow, the main Pozzolane Rosse  
3 pyroclastic units (basal fallout and main pyroclastic flow unit) and the scoria lapilli fallout  
4 deposits. Recently, the products of the Pozzolane Rosse eruption were also found in the Campo  
5 Felice basin (layer CF-V11) where it marks the local glacier advancement of the MIS 12 glacial  
6 (Giraudi and Giaccio, 2015). Pronounced glacial conditions are also recorded in the lacustrine  
7 sediments across the Pozzolene Rosse of the Sulmona basin (Regattieri et al., 2016).

8 The age of the Pozzolane Rosse eruption is well constrained by several  $^{40}\text{Ar}/^{39}\text{Ar}$ -ages. The  
9 pyroclastic products are dated to  $457\pm4$  ka at a proximal site (Karner et al., 2001), which is  
10 confirmed by the distal equivalent found in the Sulmona Basin ( $457\pm2$  ka, Giaccio et al.,  
11 2013a). These ages are further supported by  $^{40}\text{Ar}/^{39}\text{Ar}$ -ages of  $457\pm5$  ka from a lava flow below  
12 and of  $442\pm2$  ka from a relatively thin succession of fallout deposits on top (Marra et al., 2009).

13

#### 14 **4.10 OH-DP-1955 / SC5**

15 The tephra layer OH-DP-1955 (195.536–195.566 mcd) is 3 cm thick and has a sharp bottom  
16 and a diffuse top boundary. The greyish layer comprises blocky, non-vesicular glass shards and  
17 porphyric micro-pumices containing leucite crystals. The composition is mainly phonolitic to  
18 trachy-andesitic with some shards plotting in the tephri-phonolitic field (Fig. 3h, Table 1).  
19 According to the stratigraphic position, OH-DP-1955 was deposited prior to ca. 460 ka, since  
20 it is found below OH-DP-1817/Pozzolane Rosse ( $457\pm2$  ka). Proximal deposits of the active  
21 volcanoes in Italy older than 450 ka are only barely explored. From the more distal archives,  
22 the tephra layer SC5 from the Mercure Basin (Giaccio et al., 2014) shows a trachytic-andesitic  
23 to phonolitic trend similar to that of OH-DP-1955 (cf. Fig. 3h). Oxide plots (cf. Fig 6a, Suppl.  
24 I Fig. h) of major element clarify that this composition shows a linear magmatic trend and the  
25 occurrence of two different populations of tephra can be ruled out. Investigated sources for OH-  
26 DP-1955 and its potential equivalent SC5 are very limited. Sr-isotope ratios of tephra layer SC5  
27 reveal an origin from the Roccamonfina volcano (Giaccio et al., 2014).  $^{40}\text{Ar}/^{39}\text{Ar}$  dating  
28 provided an age of  $493.1\pm10.9$  ka for the SC5 tephra (Giaccio et al., 2014), which thus  
29 represents a poorly known eruption from the Roccamonfina volcano attributable to the Rio  
30 Rava stage dated between ~600 and 439 ka (Rouchon et al., 2008). Despite a similar age, a  
31 potential correlation of OH-DP-1955 with Fall B ( $490\pm4$  ka) from the Tufi Terrosi con Pomici

1 Bianche eruptive cycle (TTPB,  $499\pm3$ - $490\pm4$  ka) of the Sabatini volcanic field (Sottili et al.,  
2 2004; Marra et al., 2014) is unlikely. The composition of the Fall B deposits is somehow  
3 different, having e.g. lower FeOTOT ( $\sim 1.1$  wt.%), and CaO (1.5 wt%) but higher K<sub>2</sub>O (3.4 wt%)  
4 contents (cf. Fig. 6a, Table 1).

5

## 6 **4.11 OH-DP-2010 / Fall A**

7 OH-DP-2010 (201.034–201.049 mcd) is a reddish-brown, 1.5 cm thick layer with a sharp lower  
8 and an undulated upper boundary. It comprises morphologically different volcanic fragments,  
9 which range from non-vesicular, microlite-bearing blocky, glass shards, to medium vesicular  
10 cuspatate glass shards, and elongated vesicular micropumices. The tephri-phonolitic to phonolitic  
11 composition of tephra OH-DP-2010 (Fig. 3i, Table 1) and its characteristic high potassium  
12 content suggest an origin from the Roman province. The low Cl content of OH-DP-2010 (cf.  
13 Table 1) is typical for Middle Pleistocene Sabatini products (Giaccio et al., 2014; Palladino et  
14 al., 2014) and supports an origin from the TTPB eruptive cycle of the Sabatini volcanic district  
15 (Sottili et al., 2004; Marra et al., 2014). The major element composition and the stratigraphic  
16 position suggest that OH-DP-2010 correlates with the proximal and distal products of the oldest  
17 eruptive unit Fall A (cf. Fig. 3i; Fig. 6b). The reddish colour of OH-DP-2010 can be attributed  
18 to the reddish, terracotta-like, thermally metamorphosed clay lithics, which are a diagnostic  
19 characteristic of the proximal Fall A deposits (Sottili et al., 2004). However, the proximal  
20 deposits of Fall A apparently show a smaller compositional range (cf. Marra et al., 2014) than  
21 OH-DP-2010 and other distal archives, such as the Mercure Basin (SC3) and the Sulmona Basin  
22 (SUL 5-1c), whose correlation is corroborated by Sr-isotope analyses (Giaccio et al., 2014).  
23 Similar major element composition (cf. Table 1, Fig. 6b) suppose also a correlation of OH-DP-  
24 2010/Fall A with the Acerno tephra A9 (Petrosino et al., 2014b) and FIC-12.9 from Ficoncella  
25 site (Aureli et al., 2015).

26 Sottili et al. (2004) describe a bifurcation of the Fall A at the type section Isola Farnese at the  
27 Sabatini volcanic district with a lower sublayer A1 and an upper sublayer A2 both comprising  
28 alternating layers of white pumice and grey scoria clasts. Whereas the white pumices of these  
29 eruptive units are more evolved and trachy-phonolitic, the grey scoria clasts have a phono-  
30 tephritic to tephri-phonolitic composition (Marra et al., 2014). The reason for the wider  
31 compositional spectrum of distal Fall A deposits (e.g. OH-DP-2010, SC3) could be the lack of

1 data for the less evolved, upper grey pumices of the proximal zoned Fall A. A correlation of the  
2 older Grottarossa Pyroclastic Sequence (GPRS, Karner et al., 2001) of the Sabatini volcano  
3 (Marra et al., 2014) with the chemically similar and less evolved part of OH-DP-2010 can be  
4 excluded, since the GPRS and Fall A are temporally well distinct events, as testified by field  
5 (Sottilli et al., 2004) and  $^{40}\text{Ar}/^{39}\text{Ar}$  chronological evidence (Marra et al., 2014).

6 According to  $^{40}\text{Ar}/^{39}\text{Ar}$  dating, the lower Fall A1 has an age of  $499\pm3$  ka and the upper Fall A2  
7 has an age of  $496\pm3$  ka (Marra et al., 2014). However, unpublished age–depth interpolations  
8 from distal equivalents reveal slightly older ages, with  $510\pm3$  ka for SC3 at the Mercure Basin,  
9 and with  $502\pm4$  ka for the A9 at the Acerno Basin.

10

## 11 **4.12 OH-DP-2017 / A11/A12**

12 Tephra layer OH-DP-2017 (201.747–201.782 mcd) is whitish to yellowish, 3.5 cm thick, and  
13 has sharp bottom and top boundaries. The horizon contains highly vesicular cuspat glass shards  
14 with a varying morphology and septa thickness. The homogenous trachytic composition of OH-  
15 DP-2017 (Fig. 3j, Table 1) excludes an origin from Roman and Roccamonfina provinces, which  
16 mainly produced phonolites and tephro-phonolites during the Middle Pleistocene (cf. Giaccio  
17 et al., 2014). However, two very similar trachytic layers (A11/A12) are found in the Acerno  
18 Basin sequence (Petrosino et al., 2014b). They have a similar stratigraphic position and a similar  
19 glass chemical composition (cf. Fig. 3j+6c, Table 1) compared with OH-DP-2017 (Petrosino et  
20 al., 2014b). An unambiguous correlation of OH-DP-2017 with one of the both layers is not  
21 possible due to their indistinguishable major element composition (Table 1). Tephra SC2 from  
22 the Sulmona Basin was tentatively also correlated based on chemical affinities and its  
23 stratigraphic position with the A11/A12 (Giaccio et al., 2014). However, differences in the  
24 composition (higher FeOTOT, SiO<sub>2</sub>) do not support an unambiguous correlation of SC2 with  
25 OH-DP-2017 or A11/12 (cf. Fig 6c) and suggest that they may derive from the same source,  
26 but from different eruptions.

27 According to the geochemical characteristics, an origin of A11/12 from the Campanian area  
28 was proposed (Petrosino et al., 2014b). Proximal products of the Campanian area date back to  
29 ca. 290 ka only (Seiano Ignimbrite, Rolandi et al., 2003). Distal deposits, such as found in the  
30 Montalbano Jonico succession (around 720 ka, V5, V7, Petrosino et al., 2014c) and the  
31 Sulmona Basin (ca. 723 ka, SC1-35.30/SUL2-1, Giaccio et al., 2013b), suggest also older

1 activity of the Campanian area, which may have produced OH-DP-2017/A11/A12. Although  
2 Sr-isotope ratios indicate that tephra layer SC2 originate from the Ponza Island, the lack of  
3 Middle Pleistocene pyroclastic rocks on Ponza Island contradicts this correlation and an origin  
4 of SC2 from the Campanian area appears more likely (Giaccio et al., 2014).

5 Sanidine crystals of the Acerno tephra A11 yielded a  $^{40}\text{Ar}/^{39}\text{Ar}$  age of  $514\pm5.6$  ka (Petrosino et  
6 al., 2014b). As A12 is located only 12 cm below A11, which amounts to an age difference of a  
7 few hundred years according to the sedimentation rate between the two tephra (Petrosino et al.,  
8 2014b), the difference in age is negligible and the age of  $514\pm5.6$  ka can be transferred from  
9 the A11 to OH-DP-2017 tephra.

10

#### 11 **4.13 OH-DP-2060 / Tufo di Bagni Albule**

12 Tephra OH-DP-2060 (206.060–206.080 mcd) is a 2 cm thick, brownish-greyish tephra layer  
13 with a sharp bottom and a more diffuse upper boundary. The layer comprises mainly non-  
14 vesicular, porphyritic (leucite and sanidine), blocky glass shards. Furthermore, numerous  
15 diatoms and weathered calcite were found during microscope analysis. The characteristic K-  
16 foiditic composition (Fig. 3j, Table 1) suggests an origin from the Colli Albani volcanic district.  
17 According to the stratigraphic position of OH-DP-2060 with a presumed age older than 510 ka,  
18 it can be assigned to the Tufo del Palatino-Tufo di Bagni Albule eruptive cycle of the Colli  
19 Albani volcanic district (Karner et al., 2001; Giaccio et al., 2013a). Glass composition data are  
20 only published for the upper pyroclastic flow Tufo di Bagni Albule (TBA or Tufo di Acque  
21 Albule), which is separated by a paleosol from the lower Tufo del Palatino (TP) ignimbrite  
22 (Marra et al., 2009). A geochemical comparison of the TBA with the proximal data of the Via  
23 Tiburtina section AH-23 (within the Colli Albani volcanic district, Marra et al., 2009) and the  
24 distal equivalent found in the Sulmona Basin (SUL1-6 site 2, Giaccio et al., 2013a) reveals a  
25 good correlation with OH-DP-2060 (cf. Table 1, Fig. 6d). A relatively thick, foiditic tephra with  
26 Tufo del Palatino-Tufo di Bagni Albule products was also found in a core from the Fucino basin  
27 in the Apennine chain (Giaccio et al., 2013a). In the Intra-Apennine Carsoli Basin, a chemically  
28 very similar deposit, the so-called the Oricola tuff was found (Stoppa et al., 2005) and later  
29 correlated with TBA from the Colli Albani volcanic district based on chronological, isotopic,  
30 and major element composition affinities (Giaccio et al., 2013a). The carbonate content of the  
31 Oricola tuff (Peccerillo, 2005; Stoppa et al., 2005), which is also noticed in OH-DP-2060, is

1 typical for Colli Albani products, because the magma chambers are situated in Mesozoic  
2 limestones (Giordano et al., 2006). TP and TBA in proximal deposits indicate  
3 geochronologically indistinguishable ages of  $530 \pm 2$  and  $527 \pm 2$  ka (Marra et al., 2009), which  
4 are in a good agreement with the age obtained for the Oricola tuff (ca. 531 ka, Bosi et al., 1991).  
5 As long as no compositional glass data is available for the TP, the TBA is the most likely  
6 equivalent of OH-DP-2060 and an age of  $527 \pm 2$  ka can be assumed for this tephra.

#### 7 **4.14 Reassessing and homogenizing the age of the DEEP site tephra layers**

8 The obtained tephrochronological information from the dated equivalents of the DEEP site  
9 tephra layers were used to develop a robust chronology for the DEEP site proxy series, for both  
10 the sediment core and the borehole successions (cf. Baumgarten et al., 2015; Francke et al.,  
11 2015). For this purpose, 11 out of the presented 13 tephra layers were selected based on the  
12 strength of correlation and their geochronological reliability. Except for the Y-3, TM24a/POP2,  
13 and P-11 tephra, all ages are radiometric ages, whereas the ages of these three tephra layers  
14 were taken from the respective age-depth models. The high number of  $^{14}\text{C}$  ages above and  
15 below the Y-3 equivalent of the Tenaghi Philippon record (Albert et al. 2015) allow a reliable  
16 age interpolation, similar to the POP2 tephra from the Sulmona basin, where tephra layers above  
17 and below are precisely  $^{40}\text{Ar}/^{39}\text{Ar}$  dated (Regattieri et al., 2015). The only available  $^{40}\text{Ar}/^{39}\text{Ar}$   
18 ages of the P-11 tephra scatter between  $123 \pm 1.6$  ka and  $135 \pm 1.2$  ka. Currently, the most reliable  
19 age of P-11 is likely that obtained from the age-depth model of core LC21, which is tuned to  
20 the extensively U/Th-dated Soreq Cave speleothem record (Satow et al., 2015; Zanchetta et al.,  
21 2015).

22 In order to achieve a homogenous set of ages, all  $^{40}\text{Ar}/^{39}\text{Ar}$  ages have been recalculated relative  
23 to the same flux standard and the total  $^{40}\text{K}$  decay constant of Steiger and Jäger (1977). Since  
24 the flux standards Fish Canyon sanidine (FCs) and Alder Creek sanidine (ACs-2) are  
25 intercalibrated, all ages were recalculated to an age of 1.194 Ma for ACs, which corresponds to  
26 FCs at 28.02 Ma (Nomade et al., 2005). This choice was made because most of the published  
27 ages were calculated using these two flux standards. However, several calibrations of the  
28  $^{40}\text{Ar}/^{39}\text{Ar}$  chronometer are currently in use, which yield ages that can vary by  $\sim 1\%$  in the time  
29 range of the Pleistocene (e.g. Kuiper et al., 2008; Renne et al., 2010; Phillips and Matchan,  
30 2013). As long as it is not the purpose of this work to decipher, which calibration is the more  
31 accurate and that the implied difference in calibrated age is within the current reported fully

1 propagated uncertainties at  $2\sigma$  level, we decided to keep ages as they were published without  
2 necessarily endorsing the flux standards values used. The results are indicated in Table 2.

3 The age obtained from the suggested correlation OH-DP-0624/CF-V5 with the Pitigliano Tuff  
4 was recalculated, but not included in the age model, as the tephrostratigraphical correlation is  
5 not very robust (cf. discussion OH-DP-0624) and the  $2\sigma$  error bar is relatively large (Table 2).  
6 Furthermore, the age of the directly overlying tephra OH-DP-0617/Vico B represents a more  
7 reliable tie-point in this part of the sequence. The original/recalculated age of Fall A  $499/496 \pm 3$   
8 ka was not selected as a first order tie point for the age-depth model shown in Francke et al.  
9 (2015), because of the age-depth interpolations of the Acerno Basin and the Mercure Basin:  
10 They suggest an older age for distal Fall A, making the published age for the proximal Fall A  
11 questionable.

12 In order to obtain a first overview of the chronology of the DEEP site sequence, an age-depth  
13 plot (Fig. 7) with all tephrochronological information was created. The homogenous  
14 distribution of ages vs. depth suggests a relatively constant sedimentation rate of the DEEP site  
15 succession for the upper 247.8 m. As shown in Fig. 7, the unreliability of the  $^{40}\text{Ar}/^{39}\text{Ar}$  age of  
16 Fall A at  $496 \pm 3$  ka becomes more obvious. The tephra OH-DP-1955/SC5 dated to  $493 \pm 11$  ka  
17 is located 5.48 m above OH-DP-2010/Fall A, whilst the OH-DP-2017/A11 dated to  $514 \pm 6$  ka  
18 is located only 0.73 m below this layer. Accepting an age of  $496 \pm 3$  ka for Fall A would imply  
19 a distinct change in the sedimentation rates, with interpolated sedimentation rates of  $1.8 \text{ m ka}^{-1}$   
20 above and  $0.04 \text{ m ka}^{-1}$  below, which differ substantially from a mean sedimentation rate of  
21  $0.39 \text{ m ka}^{-1}$  for the entire sequence. However, there is no lithological evidence justifying such  
22 a conspicuous change in sedimentation rate. The radiometric dating of Fall A was done on  
23 deposits from Cava Rinaldi, which were correlated with Fall A only using trace element ratios  
24 ( $\text{Zr/Y}$  vs.  $\text{Nb/Y}$  plot) and chronological constraints, because the deposits have been too altered  
25 to use major element compositions (Marra et al., 2014). Although this method is helpful to  
26 distinguish between the different Italian provinces and between the different volcanic districts  
27 (Marra et al., 2011; Marra et al., 2014), it may be not suitable to distinguish between single  
28 eruptions, with similar composition. Moreover, the intense alteration of the deposits makes an  
29 unequivocal correlation difficult and the obtained age for Fall A is probably too young.  
30 Following the correlation of OH-DP-2010 with distal deposits of the SC3 in the Mercure and  
31 the A9 in the Acerno basin, an age of between 502 and 510 ka seems to be more likely and  
32 would be consistent with more constant sedimentation rates in the DEEP site record.

## 1   **4.15 Resulting tephrostratigraphy of the Lake Ohrid record**

2   The Middle Pleistocene Italian tephrostratigraphic framework was extended for the first time  
3   beyond Italy to the Balkan region. The 13 identified tephra layers (OH-DP-0027-2060) of the  
4   DEEP sequence link the Lake Ohrid record with numerous terrestrial and marine records of the  
5   Mediterranean region (Fig. 8) at least back to MIS13. Since the last 160 kyr are recorded in  
6   many archives, tephra layers found in Lake Ohrid of this period were also found in numerous  
7   other records and give a dense framework of tie points for this period. However, for the period  
8   between MIS 7 and MIS 11, no correlations could be established for the Lake Ohrid sequence  
9   so far, but at least 13 tephra layers between OH-DP-0624 (>160 ka) and OH-DP-1817 (<450  
10   ka) indicate activity and widespread eruptions of Italian volcanoes. On the other hand, Lake  
11   Ohrid provides a very long and continuous record of stratigraphically ordered Middle  
12   Pleistocene tephra, which represents a reference section for other discontinuous and short  
13   successions in which the stratigraphic order of tephra is unknown or not well constrained. In  
14   spite of this potential, tephrostratigraphic and volcanologic implications based on the lower part  
15   of the record below P-11 are premature, because the succession is not fully analysed and more  
16   detailed investigations are needed to complete and improve the tephrostratigraphic framework.  
17   Even still at this preliminary stage of the study, the recognition of tephra layers from volcanic  
18   provinces, which were thought to be poorly active or even inactive at the time of tephra  
19   deposition, such as the ca. 490 ka old OH-DP-1955/SC5 tephra from the Roccamonfina  
20   volcano, or the ca. 510 ka old OH-DP-2017/A11/12 tephra from the Campanian Volcanic Zone,  
21   provide insights for exploring and improve our knowledge about volcanic activity of the  
22   different provinces. Furthermore, their widespread distribution to the Balkan suggests that some  
23   of them were rather large magnitude eruptions and represent widespread marker horizons.

24   The connection to different records within the Mediterranean region also reveals the possibility  
25   to review different distribution patterns of specific eruptions, which probably will change  
26   substantially in the light of the Lake Ohrid data (e.g. OH-DP-0499/P-11/THP-TII-5).  
27   Moreover, this established tephrostratigraphic framework can be used as a powerful tool for the  
28   synchronization of different archives in order to address at very fine temporal and stratigraphic  
29   resolution relevant paleoclimate and paleoenvironmental issues (cf. Zanchetta et al., 2015).

30

1    **5 Conclusions**

2    The results of the first tephrostratigraphic study of the DEEP site succession from Lake Ohrid  
3    allowed us to recognize 34 macroscopic tephra, 12 out of which and one cryptotephra, all  
4    originating from the Italian volcanism, were correlated with their proximal or distal  
5    counterparts. Tephra layers found in the previous studies have been re-identified and were  
6    utilized as helpful markers for setting up the uppermost part of the new tephrostratigraphy of  
7    the DEEP site record. In the light of the longer tephra succession presented in this paper, the  
8    previously established correlations have been either confirmed or, in some cases, revised (e.g.  
9    OH-DP-0617/OT0701-6 and OH-DP-0624/OT0701-7). Furthermore, tephrostratigraphy was  
10   successfully applied for the succession older than the already inspected 135 ka of Lake Ohrid's  
11   history. On the whole, the following correlations are here proposed: OH-DP-0027/Mercato  
12   tephra (8.43-8.63 ka cal BP), OH-DP-0115/Y-3 (28.68-29.42 ka cal BP), OH-DP-0169/Y-5  
13   (39.6±0.1 ka), OH-DP-0404/TM24a/POP2 (102±2.4 ka), OH-DP- 0435/X-6 (109±2 ka), OH-  
14   DP-0499/P-11 (133.5±2 ka), OH-DP-0617/Vico "Ignimbrite B" (162±6 ka), OH-DP-0624/CF-  
15   V5/Pitigliano Tuff (163±22 ka), OH-DP-1817/Pozzolane Rosse (457±2 ka), OH-DP-1955/SC5  
16   (493.1±10.9 ka), OH-DP-2010/Fall A (496±3 ka), OH-DP-2017/A11/12 (511±6 ka), and OH-  
17   DP-2060/Tufo di Bagni Albule (527±2 ka).

18   The ages of 11 of the correlated tephra layers were used to contribute first order tie points to  
19   develop a robust age-depth model of the uppermost 247.8 mcd of the DEEP succession, which  
20   is a fundamental pillar for the development of the different multi-proxy paleoclimatic-  
21   environmental and evolutionary studies, which are in progress. Furthermore, this age-depth  
22   model has the potential to refine our chronological knowledge of some relevant marker tephra  
23   found in the Lake Ohrid succession (e.g. Fall A), and to provide a first chronological framework  
24   for a number of currently poorly known tephra, which, however, can be potentially found  
25   elsewhere and thus indirectly dated by simple geochemical fingerprinting. In this perspective,  
26   the data presented in this paper provide a further important step forward for extending back in  
27   time, and well beyond the current chronological limit, a robust and reliable Middle Pleistocene  
28   tephrostratigraphy in central Mediterranean area.

29

30   **Appendix A: Supplementary Material**

31   **Supplement I: Harker diagrams of established correlations of the Ohrid tephra**  
32   **layers OH-DP-0027-1955.**

1   **Supplement II: Full data set of WDS-analysis of Ohrid tephra layers OH-DP-0027-**  
2   **2060**

3   **Acknowledgements**

4   The SCOPSCO Lake Ohrid drilling campaign was funded by ICDP, the German Ministry of  
5   Higher Education and Research, the German Research Foundation, the University of Cologne,  
6   the British Geological Survey, the INGV and CNR (both Italy), and the governments of the  
7   republics of Macedonia (FYROM) and Albania. Logistic support was provided by the  
8   Hydrobiological Institute in Ohrid. Drilling was carried out by Drilling, Observation and  
9   Sampling of the Earth's Continental Crust's (DOSECC) and using the Deep Lake Drilling  
10   System (DLDS). Special thanks are due to Beau Marshall and the drilling team. Ali Skinner  
11   and Martin Melles provided immense help and advice during logistic preparation and the  
12   drilling operation.

13   **Table 1.** Average major element glass composition (normalised to 100 %) of investigated  
14   tephra layers OH-DP-0027–OH-DP-2060 of the DEEP site sequence, the discussed  
15   correlations, and the standards used for evaluation of the accuracy of the analyses. All data of  
16   the Ohrid tephra layers were obtained using a WDS, except for OH-DP-0027, which is based  
17   on EDS measurements. The “Total” is given as analytical total, and the tephra layers printed in  
18   italic are not correlated with the respective Ohrid tephra and are discussed only. The full dataset  
19   of OH-DP-0027–OH-DP-2060 is given in the Supplement 2.

20   **Table 2.** Depths and ages of tephra layers in the DEEP site succession.  $^{40}\text{Ar}/^{39}\text{Ar}$  ages with  $2\sigma$   
21   uncertainties (last column) recalculated to ACs at 1.194 Ma for, which corresponds to FCs at  
22   28.02 Ma (Nomade et al., 2005) and the total decay constant of Steiger and Jäger (1977). Tephra  
23   layers in bold are not considered for the age-depth modelling (Francke et al., 2015).

24   **Figure 1. (a)** Location of Lake Ohrid in the Mediterranean region, the Italian volcanoes, and  
25   the locations of archives mentioned in the text (1-Ficoncella Site, 2-Carsoli Basin, 3-Paganica-  
26   San Demetrio-Castelnuovo basin, 4-Campo Felice, 5-Fucino Basin, 6-Sulmona Basin, 7-  
27   PRAD1-2, 8-CM92-42, 9-RF93-77, 10-RF95-11, 11-Veliko Jezero, Island of Mljet, 12-  
28   KET8022, 13-KET8003, 14-KET8011, 15-C-45, 16-KET8004/DED8708, 17-C1202, 18-  
29   Cilento coast, 19-C106, 20-SMP1e (CE1/CD1/SMP1), 21-Acerno Basin, 22-San Gregorio  
30   Magno basin, 23-Lago Grande di Monticchio, 24-Mercure basin, 25-Montalbano Jonico  
31   succession, 26-MD90-917, 27-KET8218, 28-IN68-9, 29-IN68-5, 30-AD91-17, 31-MD90-918,  
32   32-RC9 191, 33-M25/4-12, 34-KET8222, 35-V10 69, 36-ODP 963A, 37-22M-60, 38-KC01B,

1 39-RC9 18, 40-RC9 181, 41-LC01,-42-V10 58, 43-Lesvos, 44-Tenaghi Philippon, 45-  
2 Theopetra Cave, 46-Lake Prespa). **(b)** Geological map of the Lake Ohrid catchment modified  
3 after Lindhorst et al. (2015) and the core locations from previous studies (Lz1120,  
4 Co1200/1201/1202/1262, and JO2004) and the ICDP main drill site DEEP.

5 **Figure 2.** (Litho-) Stratigraphy of the uppermost 247.8 mcd of the DEEP site sequence and the  
6 position of recognised tephra layers. Tephra layers coloured in yellow and being labeled are  
7 discussed within this paper. The thickness of tephra layers is not to scale and more detailed  
8 information about tephra thickness and appearance are provided in the text.

9 **Figure 3.** Total alkali-silica diagram after Le Bas et al., 1986 to classify and correlate the DEEP  
10 site tephra layers OH-DP-0027–OH-DP-2060 (a–j). The full dataset of the DEEP site record is  
11 given in Table 1 and in the supplementary online material. The following references were used:  
12 **a) OH-DP-0027/Pomici di Mercato:** Co1262-709 (Wagner et al., 2012), OT0702-3 (Vogel et  
13 al., 2010), PT0915-2 (Damaschke et al., 2013TM6a/TM6b (Wulf et al., 2004); MJ1/VJ1 (Jahns  
14 and van den Bogaard, 1998); KET8218 V1 (Paterne et al., 1988); IN68-9 125cm, IN68-5 259  
15 cm and RF95-11 320 cm (Calanchi and Dinelli, 2008); 190-191, 195-196 cm AD91-17  
16 (Marchini et al., 2014); 210/223cm MD90-918 (Caron et al., 2012). **b) OH-DP-0115 / Y-3:**  
17 OT0520-2; OT0700-1; OT0702-4; JO 187 (Sulpizio et al., 2010), PT0915-5, (Damaschke et  
18 al., 2013); TM15 (Wulf et al., 2004); Y-3 M25/4-12, RC9 (Keller et al., 1978; Albert et al.,  
19 2015); C7 (Paterne et al., 1988); MD90-917 920/17 (Zanchetta et al., 2008); TP 9.70 (Albert et  
20 al., 2015); A2/B2 C106/C45 (Munno and Petrosino, 2004); S19 (Munno and Petrosino, 2007).  
21 **c) OH-DP-0169 / CI/Y-5:** OT0520-3, OT0700-2, OT0701-1, OT0702-6, JO-244, PT0704-3  
22 (Sulpizio et al., 2010); Y-5 RC9 191 (Keller et al. 1978); TM-18 (Wulf et al., 2004); S-17  
23 (Munno and Petrosino, 2007); ML 2 (Margari et al., 2007); TP-CI (Lowe et al., 2012); C-13  
24 (Paterne et al., 1988); PRAD1653 (Bourne et al., 2010); I-3, (Insinga et al. 2014); LC21 4.925  
25 (Lowe et al., 2012, Satow et al. 2015); pre-CI deposits (Tomlinson et al., 2012).  
**d) OH-DP-0404 / TM24a POP2 :** OT-0702-8 (Vogel et al., 2010); TM24a (Wulf et al., 2004; Wulf et al.,  
26 2012); POP2 (Regattieri et al., 2015); CM92-42 (710 cm), RF93-77 (797 cm) (Calanchi and  
27 Dinelli, 2008). **e) OH-DP-0435 / X-6:** OT0702-9 (Vogel et al., 2010), JO-575 (Caron et al.,  
28 2010); X-6 (Keller et al., 1978); C-31 (Paterne et al., 2008); TM27 (Wulf et al., 2012); POP4  
29 (Regattieri et al., 2015); PRAD-2812 (Bourne et al., 2015); I-9 (Insinga et al., 2014); S10  
30 (Munno and Petrosino, 2007); SM1-2/SA (Marciano et al., 2008); CIL2 (Giaccio et al., 2012);  
31 t1 (Iorio et al., 2014). **f) OH-DP-0499 / P-11:** OT0702-10 (Vogel et al., 2010), JO-941 (Caron

et al., 2010); P-11 (Paterne et al., 2008); ODP2-4 (Tamburrino et al., 2012); ML5 (Margari et al., 2007); THP-TII5 (Karkanas et al., 2015); LC21 10.345 (Satow et al., 2015). **f) OH-DP-0617 / Vico “Ignimbrite B”:** OT0701-6 (Sulpizio et al., 2010); CF-V4 (Graudi et al., 2011); Vico B (Graudi et al. 2011). **g) OH-DP-0624 / CF-V5/ PRAD3225:** OT0701-7 (Sulpizio et al., 2010); PRAD3225 (Bourne et al., 2015); CF-V5 tephra (Graudi and Giaccio, 2015); C-42 (Paterne et al., 2008). **h) OH-DP-1817 / Pozzolane Rosse:** AH-20-PRa (Marra et al., 2009); basal fallout (Freda et al., 2010); Paganica-Raiano-Sulmona (Giaccio et al., 2013a); CF-V11 (Graudi and Giacco, 2015). **h) OH-DP-1955 / SC5:** SC5 (Giaccio et al., 2014); Fall B (Marra et al., 2014). **i) OH-DP-2010 / Fall A:** Proximal Fall A (Marra et al., 2014); SC3 and SUL 5-1c (Giaccio et al., 2014); A9 (Petrosino et al., 2014b); FIC-12.9 (Aureli et al., 2015). **j) OH-DP-2017/ A11/A12:** A11/12 (Petrosino et al., 2014b); SC2 (Giaccio et al., 2014).

**Figure 4.**  $\text{Al}_2\text{O}_3$ - $\text{FeO}_{\text{TOT}}$  diagram for classification of comendites and pantellerites according to MacDonald (1974). Tephra OH-DP-0499 and most of the other P-11 equivalents show the typical bimodal chemical composition of P-11, except for the very distal equivalents LC21 10.345 and THP-TII5, which only have a pantelleritic part (see text for data references).

**Figure 5.** Harker diagrams of tephra layers OH-DP-0617-OH-DP-1817 and their discussed equivalents. For references of correlated tephra layers, see text, additional Harker diagrams for OH-DP-1817 can be found in the Supplement I Fig. g.

**Figure 6.** Harker diagrams of tephra layers OH-DP-1955-OH-DP-2060 and their discussed equivalents. For references of correlated tephra layers, see text, additional Harker diagrams for OH-DP-1955 can be found in the Supplement I Fig. h.

**Figure 7.** Age-depth plot for the selected DEEP site tephra layers. The ages of the tephra layers are based on recalculation of existing  $^{40}\text{Ar}/^{39}\text{Ar}$  ages (Table 2) or according to published data for non  $^{40}\text{Ar}/^{39}\text{Ar}$  ages. Chronological tie points were interpolated on a linear basis (blue line). The dotted lines in the insert indicate a suspicious change in the sedimentation rate for a different age of the Fall A tephra.

**Figure 8.** Tephrostratigraphic framework of Lake Ohrid and selected archives of the last 637 kyrs corresponding to MIS16. The dashed parts of the archive columns indicate the part of the existing record, where no tephrostratigraphic information are available at present. The following archives and tephra layers are presented: Lago Grande di Monticchio (LgdM, Wulf et al. 2004, 2012), Siciliy Channel: ODP963 (Tamburino et al. 2012), Tyrrhenian Sea:

1 KET8004/DED8708, KET8003,-8011,8022 (C-7,-13,-31,-42, Paterne et al., 1988, 2008);  
2 C1202 (t1, Iorio et al. 2014); C45/106 (A2/B2, Munno and Petrosino, 2004), Adriatic Sea:  
3 KET8218 (V-1, Paterne et al., 1988), IN68-9, IN68-5, RF95-11, CM92-42, RF93-77  
4 (\*125/259/320, 710/797 Calanchi and Dinelli, 2008); AD91-17 (“190-191/195-196, Marchini  
5 et al., 2014); MD90-917 (920-17, Zanchetta et al., 2008); MD90-918 (#210/223 Caron et al.  
6 2012); PRAD1-2 (PRAD 1653, 2812, 3225, Bourne et al., 2010, 2015), Ionian Sea: MD25/4-12  
7 (Y-3, Albert et al., 2015); RC9-191, 22M-60, V10 69 (Y-3, Y-5, X-6, Keller et al., 1978); KET-  
8 8222 (C-31, P-11, Paterne et al., 2008); KC01B (I-3, I-9, Insinga et al. 2014), Levantine Sea:  
9 RC9-183, RC9-181 (Y-5, Keller et al., 1978), Aegean Sea: V10-58 (Y-5, Keller et al., 1978);  
10 LC01 (4.925, 10.345, Satow et al., 2015), Tenaghi Philippon: (TP9.70, Albert et al., 2015; CI,  
11 Lowe et al., 2012), San Gregorio Magno Basin (Munno and Petrosino, 2007), Campo Felice  
12 basin (Giraudi et al., 2011, 2015), Sulmona basin (Giaccio et al. 2013b, Regattieri et al., 2015),  
13 Acerno basin (Petrosino et al., 2013b), Mercure basin (Giaccio et al., 2014).

14

## 15 **6 References**

- 16 Aksu, A. E., Jenner, G., Hiscott, R. N., and Isler, E. B.: Occurrence, stratigraphy and  
17 geochemistry of Late Quaternary tephra layers in the Aegean Sea and the Marmara Sea, Mar.  
18 Geol., 252, 174-192, 2008.
- 19 Albert, P. G., Hardiman, M., Keller, J., Tomlinson, E. L., Smith, V. C., Bourne, A. J., Wulf, S.,  
20 Zanchetta, G., Sulpizio, R., Muller, U. C., Pross, J., Ottolini, L., Matthews, I. P., Blockley, S.  
21 P. E., and Menzies, M. A.: Revisiting the Y-3 teprostratigraphic marker: a new diagnostic  
22 glass geochemistry, age estimate, and details on its climastratigraphical context, Quaternary  
23 Sci. Rev., 118, 105-121, 2015.
- 24 Le Bas, M. J. L., Maitre, R. W. L., Streckeisen, A., and Zanettin, B.: A Chemical Classification  
25 of Volcanic Rocks Based on the Total Alkali-Silica Diagram, J. Petrol., 27, 745-750, 1986.
- 26 Baumgarten, H., Wonik, T., Tanner, D. C., Francke, A., Wagner, B., Zanchetta, G., Sulpizio,  
27 R., Giaccio, B., and Nomade, S.: Age depth-model for the past 630 ka in Lake Ohrid  
28 (Macedonia/Albania) based on cyclostratigraphic analysis of downhole gamma ray data,  
29 Biogeosciences Discussions, 12, 7671-7703, 2015.
- 30 Bear, A. N., Cas, R. A. F., and Giordano, G.: Variations in eruptive style and depositional  
31 processes associated with explosive, phonolitic composition, caldera-forming eruptions: The  
32 151 ka Sutri eruption, Vico Caldera, central Italy, J. Volcanol. Geoth. Res., 184, 225-255, 2009.
- 33 Bosi, C., Locardi, E., and Villa, I.: Il distretto magmatico abruzzese, Riassunti workshop  
34 “Evoluzione dei bacini Neogenici e loro rapporti con il magmatismo Plio-Quaternario nell’area  
35 Tosco-Laziale”, Pisa 12-13 June 1991, 68-69, 1991.
- 36 Bourne, A. J., Lowe, J. J., Trincardi, F., Asioli, A., Blockley, S. P. E., Wulf, S., Matthews, I.  
37 P., Piva, A., and Vigliotti, L.: Distal tephra record for the last ca 105,000 years from core PRAD

- 1 1-2 in the central Adriatic Sea implications for marine tephrostratigraphy, Quaternary Sci. Rev.,  
2 29, 3079-3094, 2010.
- 3 Bourne, A. J., Albert, P. G., Matthews, I. P., Trincardi, F., Wulf, S., Asioli, A., Blockley, S. P.  
4 E., Keller, J., and Lowe, J. J.: Tephrochronology of core PRAD 1-2 from the Adriatic Sea:  
5 insights into Italian explosive volcanism for the period 200-80 ka, Quaternary Sci. Rev., 116,  
6 28-43, 2015.
- 7 Calanchi, N. and Dinelli, E.: Tephrostratigraphy of the last 170 ka in sedimentary successions  
8 from the Adriatic Sea, J. Volcanol. Geoth. Res., 177, 81-95, 2008.
- 9 Calanchi, N., Cattaneo, A., Dinelli, E., Gasparotto, G., and Lucchini, F.: Tephra layers in Late  
10 Quaternary sediments of the central Adriatic Sea, Mar. Geol., 149, 191-209, 1998.
- 11 Caron, B., Sulpizio, R., Zanchetta, G., Siani, G., and Santacroce, R.: The Late Holocene to  
12 Pleistocene tephrostratigraphic record of Lake Ohrid (Albania), Comptes Rendus Geoscience,  
13 342, 453-466, 2010.
- 14 Caron, B., Siani, G., Sulpizio, R., Zanchetta, G., Paterne, M., Santacroce, R., Tema, E., and  
15 Zanella, E.: Late Pleistocene to Holocene tephrostratigraphic record from the Northern Ionian  
16 Sea, Mar. Geol., 311, 41-51, 2012.
- 17 Civetta, L., Cornette, Y., Crisci, G., Gillot, P. Y., Orsi, G., and Requejo, C. S.: Geology,  
18 Geochronology and Chemical Evolution of the Island of Pantelleria, Geol. Mag., 121, 541-562,  
19 1984.
- 20 Civetta, L., Orsi, G., Pappalardo, L., Fisher, R. V., Heiken, G., and Ort, M.: Geochemical  
21 zoning, mingling, eruptive dynamics and depositional processes - The Campanian Ignimbrite,  
22 Campi Flegrei caldera, Italy, J. Volcanol. Geoth. Res., 75, 183-219, 1997.
- 23 Damaschke, M., Sulpizio, R., Zanchetta, G., Wagner, B., Bohm, A., Nowaczyk, N.,  
24 Rethemeyer, J., and Hilgers, A.: Tephrostratigraphic studies on a sediment core from Lake  
25 Prespa in the Balkans, Clim. Past, 9, 267-287, 2013.
- 26 De Vivo, B., Rolandi, G., Gans, P. B., Calvert, A., Bohrson, W. A., Spera, F. J., and Belkin, H.  
27 E.: New constraints on the pyroclastic eruptive history of the Campanian volcanic Plain (Italy),  
28 Miner. Petrol., 73, 47-65, 2001.
- 29 Deino, A. L., Southon, J., Terrasi, F., Campajola, L., and Orsi, G.:  $^{14}\text{C}$  and  $^{40}\text{Ar}/^{39}\text{Ar}$  Dating of  
30 the Campanian Ignimbrite, Phlegrae Fields, Italy, 8th International Conference on  
31 Geochronology, Cosmochronology and Isotope Geology, Berkeley, CA, USA, Abstracts US  
32 Geol. Surv. Circ., 1107, 77, 1994.
- 33 Di Vito, M. A., Sulpizio, R., Zanchetta, G., and D'Orazio, M.: The late Pleistocene pyroclastic  
34 deposits of the Campanian Plain: New insights into the explosive activity of Neapolitan  
35 volcanoes, J. Volcanol. Geoth. Res., 177, 19-48, 2008.
- 36 Druitt, T. H., Brenchley, P. J., Gokten, Y. E., and Francaviglia, V.: Late Quaternary Rhyolitic  
37 Eruptions from the Acigol Complex, Central Turkey, J. Geol. Soc. London, 152, 655-667, 1995.
- 38 Druitt, T. H., Edwards, L., Mellors, R., Pyle, D., Sparks, R., Lanphere, M., Davies, M., and  
39 Barreirio, B.: Santorini volcano, Geological Society, London, Memoirs, 19, 1-161, 1999.
- 40 Francke, A., Wagner, B., Just, J., Leicher, N., Gromig, R., Baumgarten, H., Vogel, H., Lacey,  
41 J. H., Sadori, L., Wonik, T., Leng, M. J., Zanchetta, G., Sulpizio, R., and Giaccio, B.:  
42 Sedimentological processes and environmental variability at Lake Ohrid (Macedonia, Albania)

- 1 between 640 ka and present day, *Biogeosciences Discuss.*, 12, 15111–15156, 2015,  
2 <http://www.biogeosciences-discuss.net/12/15111/2015/>.
- 3 Freda, C., Gaeta, M., Giaccio, B., Marra, F., Palladino, D. M., Scarlato, P., and Sottili, G.: CO<sub>2</sub>-  
4 driven large mafic explosive eruptions: the Pozzolane Rosse case study from the Colli Albani  
5 Volcanic District (Italy), *B. Volcanol.*, 73, 241-256, 2011.
- 6 Galli, P., Giaccio, B., and Messina, P.: The 2009 Central Italy earthquake seen through 0.5 Myr-  
7 long tectonic history of the L'Aquila faults system, *Quaternary Sci. Rev.*, 29, 3768-3789, 2010.
- 8 Giaccio, B., Nomade, S., Wulf, S., Isaia, R., Sottili, G., Cavuoto, G., Galli, P., Messina, P.,  
9 Sposato, A., Sulpizio, R., and Zanchetta, G.: The late MIS 5 Mediterranean tephra markers: a  
10 reappraisal from peninsular Italy terrestrial records, *Quaternary Sci. Rev.*, 56, 31-45, 2012.
- 11 Giaccio, B., Arienzio, I., Sottili, G., Castorina, F., Gaeta, M., Nomade, S., Galli, P., and Messina,  
12 P.: Isotopic (Sr-Nd) and major element fingerprinting of distal tephras: an application to the  
13 Middle-Late Pleistocene markers from the Colli Albani volcano, central Italy, *Quaternary Sci.*  
14 *Rev.*, 67, 190-206, 2013a.
- 15 Giaccio, B., Castorina, F., Nomade, S., Scardia, G., Voltaggio, M., and Sagnotti, L.: Revised  
16 Chronology of the Sulmona Lacustrine Succession, Central Italy, *J. Quaternary Sci.*, 28, 545-  
17 551, 2013b.
- 18 Giaccio, B., Isaia, R., Fedele, F. G., Di Canzio, E., Hoffecker, J., Ronchitelli, A., Sinitsyn, A.  
19 A., Anikovich, M., Lisitsyn, S. N., and Popov, V. V.: The Campanian Ignimbrite and Codola  
20 tephra layers: Two temporal/stratigraphic markers for the Early Upper Palaeolithic in southern  
21 Italy and eastern Europe, *J. Volcanol. Geoth. Res.*, 177, 208-226, 2008.
- 22 Giaccio, B., Galli, P., Peronace, E., Arienzio I., Nomade, S., Cavinato, G. P., Mancini, M.,  
23 Messina, P., and Sottili, G.: A 560-440 ka tephra record from the Mercure Basin, Southern  
24 Italy: volcanological and tephrostratigraphic implications, *J. Quaternary Sci.*, 29, 232-248,  
25 2014.
- 26 Giaccio, B., Regattieri, E., Zanchetta, G., Nomade, S., Renne, P. R., Sprain, C.J., Drysdale,  
27 R.N., Tzedakis, P. C., Messina, P., Scardia, G., Sposato, A., and Bassinot, F.: Duration and  
28 dynamics of the best orbital analogue to the present interglacial, *Geology* 43, 603–606, 2015.
- 29 Giordano, G., De Benedetti, A. A., Diana, A., Diano, G., Gaudioso, F., Marasco, F., Miceli, M.,  
30 Mollo, S., Cas, R. A. F., and Funiciello, R.: The Colli Albani mafic caldera (Roma, Italy):  
31 Stratigraphy, structure and petrology, *J. Volcanol. Geoth. Res.*, 155, 49-80, 2006.
- 32 Giraudi, C., Bodrato, G., Lucchi, M. R., Cipriani, N., Villa, I. M., Giaccio, B., and Zuppi, G.  
33 M.: Middle and late Pleistocene glaciations in the Campo Felice Basin (central Apennines,  
34 Italy), *Quaternary Res.*, 75, 219-230, 2011.
- 35 Giraudi, C. and Giaccio, B.: Middle Pleistocene glaciations in the Apennines, Italy: new  
36 chronological data and preservation of the glacial record, *Geological Society, London, Special*  
37 *Publications*, 433, 2015.
- 38 Grant, K. M., Rohling, E. J., Bar-Matthews, M., Ayalon, A., Medina-Elizalde, M., Ramsey, C.  
39 B., Satow, C., and Roberts, A. P.: Rapid coupling between ice volume and polar temperature  
40 over the past 150,000 years, *Nature*, 491, 744-747, 2012.
- 41 Hamann, Y., Wulf, S., Ersoy, O., Ehrmann, W., Aydar, E., and Schmiedl, G.: First evidence of  
42 a distal early Holocene ash layer in Eastern Mediterranean deep-sea sediments derived from the  
43 Anatolian volcanic province, *Quaternary Res.*, 73, 497-506, 2010.

- 1 Hoffmann, N., Reicherter, K., Fernandez-Steeger, T., and Grutzner, C.: Evolution of ancient  
2 Lake Ohrid: a tectonic perspective, *Biogeosciences*, 7, 3377-3386, 2010.
- 3 Incarbona, A., Bonomo, S., Di Stefano, E., Zgozi, S., Essarbout, N., Talha, M., Tranchida, G.,  
4 Bonanno, A., Patti, B., Placenti, F., Buscaino, G., Cuttitta, A., Basilone, G., Bahri, T., Massa,  
5 F., Censi, P., and Mazzola, S.: Calcareous nannofossil surface sediment assemblages from the  
6 Sicily Channel (central Mediterranean Sea): Palaeoceanographic implications, *Mar. Micropaleontol.*, 67, 297-309, 2008.
- 7 Insinga, D. D., Tamburrino, S., Lirer, F., Vezzoli, L., Barra, M., De Lange, G. J., Tiepolo, M.,  
8 Vallefuoco, M., Mazzola, S., and Sprovieri, M.: Tephrochronology of the astronomically-tuned  
9 KC01B deep-sea core, Ionian Sea: insights into the explosive activity of the Central  
10 Mediterranean area during the last 200 ka, *Quaternary Sci. Rev.*, 85, 63-84, 2014.
- 11 Iorio, M., Liddicoat, J., Budillon, F., Incoronato, A., Coe, R. S., Insinga, D. D., Cassata, W. S.,  
12 Lubritto, C., Angelino, A., and Tamburrino, S.: Combined palaeomagnetic secular variation  
13 and petrophysical records to time-constrain geological and hazardous events: An example from  
14 the eastern Tyrrhenian Sea over the last 120 ka, *Global and Planet. Change*, 113, 91-109, 2014.
- 15 Jahns, S. and van den Bogaard, C.: New palynological and tephrostratigraphical investigations  
16 of two salt lagoons on the island of Mljet, south Dalmatia, Croatia, *Veg. His. Archaeobot.*, 7,  
17 219-234, 1998.
- 18 Karkanas, P., White, D., Lane, C. S., Stringer, C., Davies, W., Cullen, V. L., Smith, V. C.,  
19 Ntinou, M., Tsartsidou, G., and Kyparissi-Apostolika, N.: Tephra correlations and climatic  
20 events between the MIS6/5 transition and the beginning of MIS3 in Theopetra Cave, central  
21 Greece, *Quaternary Sci. Rev.*, 118, 170-181, 2015.
- 22 Karner, D. B., Juvigne, E., Brancaccio, L., Cinque, A., Ermolli, E. R., Santangelo, N.,  
23 Bernasconi, S., and Lirer, L.: A potential early middle Pleistocene tephrostratotype for the  
24 Mediterranean basin: the Vallo Di Diano, Campania, Italy, *Global and Planet. Change*, 21, 1-  
25 15, 1999.
- 26 Karner, D. B., Marra, F., and Renne, P. R.: The history of the Monti Sabatini and Alban Hills  
27 volcanoes: groundwork for assessing volcanic-tectonic hazards for Rome, *J. Volcanol. Geoth.  
28 Res.*, 107, 185-219, 2001.
- 29 Keller, J., Ryan, W. B. F., Ninkovich, D., and Altherr, R.: Explosive volcanic activity in the  
30 Mediterranean over the past 200,000 yr as recorded in deep-sea sediments, *Geol. Soc. Am.  
31 Bull.*, 89, 591-604, 1978.
- 32 Keller, J., Gertisser, R., Reusser, E., and Dietrich, V.: Pumice deposits of the Santorini Lower  
33 Pumice 2 eruption on Anafi island, Greece: Indications for a Plinian event of exceptional  
34 magnitude, *J. Volcanol. Geoth. Res.*, 278, 120-128, 2014.
- 35 Kraml, M.: Laser-40Ar/39Ar-Datierungen an distalen marinen Tephren des jung-quartären  
36 mediterranen Vulkanismus (Ionisches Meer, METEOR-Fahrt 25/4), Ph.D., Albert-Ludwigs-  
37 Universität Freiburg i.Br., 216 pp., 1997.
- 38 Kuiper, K. F., Deino, A., Hilgen, F. J., Krijgsman, W., Renne, P. R., and Wijbrans, J. R.:  
39 Synchronizing rock clocks of Earth history, *Science*, 320, 500-504, 2008.
- 40 Laskar, J., Robutel, P., Joutel, F., Gastineau, M., Correia, A. C. M., and Levrard, B.: A long-  
41 term numerical solution for the insolation quantities of the Earth, *Astron. Astrophys.*, 428, 261-  
42 285, 2004.

- 1 Laurenzi, M. A. and Villa, I.: 40Ar/39Ar chronostratigraphy of Vico ignimbrites, Period.  
2 Mineral., 56, 285-293, 1987.
- 3 Lindhorst, K., Krastel, S., Reicherter, K., Stipp, M., Wagner, B., and Schwenk, T.: Sedimentary  
4 and tectonic evolution of Lake Ohrid (Macedonia/Albania), Basin Research, 27, 84-101, 2015.
- 5 Lisiecki, L. E. and Raymo, M. E.: A Pliocene-Pleistocene stack of 57 globally distributed  
6 benthic  $\delta^{18}\text{O}$  records, Paleoceanography, 20, PA1003, doi:10.1029/2004PA001071, 2005.
- 7 Lourens, L. J.: Revised tuning of Ocean Drilling Program Site 964 and KC01B (Mediterranean)  
8 and implications for the  $\delta^{18}\text{O}$ , tephra, calcareous nannofossil, and geomagnetic reversal  
9 chronologies of the past 1.1 Myr, Paleoceanography, 19, PA3010, doi:10.1029/2003PA000997,  
10 2004.
- 11 Lowe, D.J., Tephrochronology and its application: a review. Quaternary Geochronology 6, 107-  
12 153, 2011.
- 13 Lowe, J., Barton, N., Blockley, S., Ramsey, C. B., Cullen, V. L., Davies, W., Gamble, C., Grant,  
14 K., Hardiman, M., Housley, R., Lane, C. S., Lee, S., Lewis, M., MacLeod, A., Menzies, M.,  
15 Müller, W., Pollard, M., Price, C., Roberts, A. P., Rohling, E. J., Satow, C., Smith, V. C.,  
16 Stringer, C. B., Tomlinson, E. L., White, D., Albert, P., Arienzo, I., Barker, G., Borić, D.,  
17 Carandente, A., Civetta, L., Ferrier, C., Guadelli, J.-L., Karkanas, P., Koumouzelis, M., Müller,  
18 U. C., Orsi, G., Pross, J., Rosi, M., Shalamanov-Korobar, L., Sirakov, N., and Tzedakis, P. C.:  
19 Volcanic ash layers illuminate the resilience of Neanderthals and early modern humans to  
20 natural hazards, Proc Natl Acad Sci, 109, 13532-13537, 2012.
- 21 Lustrino, M., Duggen, S., and Rosenberg, C. L.: The Central-Western Mediterranean:  
22 Anomalous igneous activity in an anomalous collisional tectonic setting, Earth-Sci. Rev., 104,  
23 1-40, 2011.
- 24 MacDonald, R.: Nomenclature and petrochemistry of the peralkaline oversaturated extrusive  
25 rocks, B. Volcanol., 38, 498-516, 1974.
- 26 Mahood, G. A. and Hildreth, W.: Geology of the peralkaline volcano at Pantelleria, Strait of  
27 Sicily, B. Volcanol., 48, 143-172, 1986.
- 28 Marchini, G., Zanchetta, G., Santacroce, R., Vigliotti, L., Capotondi, L., and Sulpizio, R.:  
29 Tephrostratigraphy of marine core AD91-17 (Adriatic Sea) Revised, Alpine and Mediterranean  
30 Quaternary, 27, 77-84, 2014.
- 31 Marciano, R., Munno, R., Petrosino, P., Santangelo, N., Santo, A., and Villa, I.: Late quaternary  
32 tephra layers along the Cilento coastline (southern Italy), J. Volcanol. Geoth. Res., 177, 227-  
33 243, 2008.
- 34 Margari, V., Pyle, D. M., Bryant, C., and Gibbard, P. L.: Mediterranean tephra stratigraphy  
35 revisited: Results from a long terrestrial sequence on Lesvos Island, Greece, J. Volcanol. Geoth.  
36 Res., 163, 34-54, 2007.
- 37 Marianelli, P. and Sbrana, A.: Risultati di misure di standard di minerali e di vetri naturali in  
38 microanalisi a dispersione di energia, Atti della Societa Toscana di Scienze Naturali Memorie  
39 Serie A, 105, 57-63, 1998.
- 40 Marianelli, P., Sbrana, A., and Proto, M.: Magma chamber of the Campi Flegrei supervolcano  
41 at the time of eruption of the Campanian Ignimbrite, Geology, 34, 937-940, 2006.

- 1 Marra, F., Karner, D. B., Freda, C., Gaeta, M., and Renne, P.: Large mafic eruptions at Alban  
2 Hills Volcanic District (Central Italy): Chronostratigraphy, petrography and eruptive behavior,  
3 J. Volcanol. Geoth. Res., 179, 217-232, 2009.
- 4 Marra, F., Deocampo, D., Jackson, M. D., and Ventura, G.: The Alban Hills and Monti Sabatini  
5 volcanic products used in ancient Roman masonry (Italy): An integrated stratigraphic,  
6 archaeological, environmental and geochemical approach, Earth-Sci. Rev., 108, 115-136, 2011.
- 7 Marra, F., Sottili, G., Gaeta, M., Giaccio, B., Jicha, B., Masotta, M., Palladino, D. M., and  
8 Deocampo, D. M.: Major explosive activity in the Monti Sabatini Volcanic District (central  
9 Italy) over the 800-390 ka interval: geochronological-geochemical overview and  
10 tephrostratigraphic implications, Quaternary Sci. Rev., 94, 74-101, 2014.
- 11 Matter, M., Anselmetti, F. S., Jordanoska, B., Wagner, B., Wessels, M., and Wüest, A.:  
12 Carbonate sedimentation and effects of eutrophication observed at the Kališta subaqueous  
13 springs in Lake Ohrid (Macedonia), Biogeosciences, 7, 3755-3767, 2010.
- 14 Matzinger, A., Jordanoski, M., Veljanoska-Sarafiloska, E., Sturm, M., Muller, B., and Wuest,  
15 A.: Is Lake Prespa jeopardizing the ecosystem of ancient Lake Ohrid?, Hydrobiologia, 553, 89-  
16 109, 2006a.
- 17 Matzinger, A., Spirkovski, Z., Patceva, S., and Wuest, A.: Sensitivity of ancient Lake Ohrid to  
18 local anthropogenic impacts and global warming, J.of Great Lakes Res., 32, 158-179, 2006b.
- 19 Mele, D., Sulpizio, R., Dellino, P., and La Volpe, L.: Stratigraphy and eruptive dynamics of a  
20 pulsating Plinian eruption of Somma-Vesuvius: the Pomici di Mercato (8900 years B.P.), B.  
21 Volcanol., 73, 257-278, 2011.
- 22 Munno, R. and Petrosino, P.: New constraints on the occurrence of Y-3 Upper Pleistocene tephra  
23 marker layer in the Tyrrhenian Sea, Il Quaternario, 17, 11-20, 2004.
- 24 Munno, R. and Petrosino, P.: The late Quaternary tephrostratigraphical record of the San  
25 Gregorio Magno Basin (Southern Italy), J. Quaternary Sci., 22, 247-266, 2007.
- 26 Narcisi, B. and Vezzoli, L.: Quaternary stratigraphy of distal tephra layers in the Mediterranean  
27 - an overview, Global and Planet. Change, 21, 31-50, 1999.
- 28 Nomade, S., Renne, P., Vogel, N., Deino, A., Sharp, W., Becker, T., Jaouni, A., and Mundil,  
29 R.: Alder Creek sanidine (ACs-2): a Quaternary 40 Ar/39 Ar dating standard tied to the Cobb  
30 Mountain geomagnetic event, Chem. Geol., 218, 315-338, 2005.
- 31 Orsi, G., DeVita, S., and diVito, M.: The restless, resurgent Campi Flegrei nested caldera  
32 (Italy): Constraints on its evolution and configuration, J. Volcanol. Geoth. Res., 74, 179-214,  
33 1996.
- 34 Palladino, D. M., Simei, S., Sottili, G., and Trigila, R.: Integrated approach for the  
35 reconstruction of stratigraphy and geology of Quaternary volcanic terrains: An application to  
36 the Vulsini Volcanoes (Central Italy), Geol. S. Am. S., 464, 63-84, 2010.
- 37 Palladino, D. M., Gaeta, M., Giaccio, B., and Sottili, G.: On the anatomy of magma chamber  
38 and caldera collapse: the example of trachy-phonolitic explosive eruptions of the Roman  
39 Province (central Italy). J. Volcanol. Geotherm. Res. 281, 12–26, 2014. Pappalardo, L., Civetta,  
40 L., de Vita, S., Di Vito, M., Orsi, G., Carandente, A., and Fisher, R. V.: Timing of magma  
41 extraction during the Campanian Ignimbrite eruption (Campi Flegrei Caldera), J. Volcanol.  
42 Geoth. Res., 114, 479-497, 2002.

- 1 Paterne, M., Guichard, F., Labeyrie, J., Gillot, P. Y., and Duplessy, J. C.: Tyrrhenian Sea  
2 Tephrochronology of the Oxygen Isotope Record for the Past 60,000 Years, *Mar. Geol.*, 72,  
3 259-285, 1986.
- 4 Paterne, M., Guichard, F., and Labeyrie, J.: Explosive activity of the South Italian volcanoes  
5 during the past 80,000 years as determined by marine tephrochronology, *J. Volcanol. Geoth.*  
6 Res., 34, 153-172, 1988.
- 7 Paterne, M., Guichard, F., Duplessy, J. C., Siani, G., Sulpizio, R., and Labeyrie, J.: A 90,000–  
8 200,000 yrs marine tephra record of Italian volcanic activity in the Central Mediterranean Sea,  
9 *J. Volcanol. Geoth. Res.*, 177, 187-196, 2008.
- 10 Peccerillo, A.: Plio-Quaternary Volcanism in Italy: Petrology, Geochemistry, Geodynamics,  
11 Springer-Verlag Berlin Heidelberg, Berlin, 2005.
- 12 Petrosino, P., Ermolli, E. R., Donato, P., Jicha, B., Robustelli, G., and Sardella, R.: Using  
13 Tephrochronology and palynology to date the MIS 13 lacustrine sediments of the Mercure  
14 Basin (Southern Apennines – Italy), *Italian Journal of Geosciences*, 133, 169-186, 2014a.
- 15 Petrosino, P., Jicha, B. R., Mazzeo, F. C., and Russo Ermolli, E.: A high resolution  
16 tephrochronological record of MIS 14–12 in the Southern Apennines (Acerno Basin, Italy), *J.*  
17 *Volcanol. Geoth. Res.*, 274, 34-50, 2014b.
- 18 Petrosino, P., Jicha, B. R., Mazzeo, F. C., Ciaranfi, N., Girone, A., Maiorano, P., and Marino,  
19 M.: The Montalbano Jonico marine succession: An archive for distal tephra layers at the Early–  
20 Middle Pleistocene boundary in southern Italy, *Quatern. Int.*, 383, 89-103, 2015.
- 21 Phillips, D. and Matchan, E.: Ultra-high precision  $^{40}\text{Ar}/^{39}\text{Ar}$  ages for Fish Canyon Tuff and  
22 Alder Creek Rhyolite sanidine: New dating standards required?, *Geochim. et Cosmochim. Ac.*,  
23 121, 229-239, 2013.
- 24 Pross, J., Tzedakis, P. C., Schmiedl, G., Christianis, K., Hooghiemstra, H., Müller, C., Ulrich,  
25 K., Ulrich, K., and Stavros, M.: Tenaghi Philippon (Greece) Revisited: Drilling a Continuous  
26 Lower-Latitude Terrestrial Climate archive of the Last 250,000 Years, *Scientific Drilling*, 5,  
27 44-46, 2007.
- 28 Pyle, D. M., Ricketts, G. D., Margari, V., van Andela, T. H., Sinitzyn, A. A., Praslov, N. D.,  
29 and Lisitsyn, S.: Wide dispersal and deposition of distal tephra during the Pleistocene  
30 'Campanian Ignimbrite/Y5' eruption, Italy, *Quaternary Sci. Rev.*, 25, 2713-2728, 2006.
- 31 Regattieri, E., Giaccio, B., Zanchetta, G., Drysdale, R. N., Galli, P., Nomade, S., Peronace, E.,  
32 and Wulf, S.: Hydrological variability over the Apennines during the Early Last Glacial  
33 precession minimum, as revealed by a stable isotope record from Sulmona basin, Central Italy,  
34 *J. Quaternary Sci.*, 30, 19-31, 2015.
- 35 Regattieri, E., Giaccio, B., Galli, P., Nomade, S., Peronace, E., Messina P., Sposato, A., Boschi,  
36 C. and Gemelli, M.: A multi-proxy record of MIS 11-12 deglaciation and glacial MIS 12  
37 instability from the Sulmona Basin (central Italy), *Quaternary Sci Rev.* 132, 129-145, 2016.
- 38 Reicherter, K., Hoffmann, N., Lindhorst, K., Krastel, S., Fernández-Steeger, T., Grützner, C.,  
39 and Wiatr, T.: Active basins and neotectonics: morphotectonics of the Lake Ohrid Basin  
40 (FYROM and Albania), *Z. Dtsch. Ges. Geowiss.*, 162, 217-234, 2011.
- 41 Renne, P. R., Mundil, R., Balco, G., Min, K., and Ludwig, K. R.: Joint determination of  $40\text{K}$   
42 decay constants and  $40\text{Ar}*/^{40}\text{K}$  for the Fish Canyon sanidine standard, and improved accuracy  
43 for  $40\text{Ar}/^{39}\text{Ar}$  geochronology, *Geochim. Cosmochim. Ac.*, 74, 5349-5367, 2010.

- 1 Robertson, A. and Shallo, M.: Mesozoic–Tertiary tectonic evolution of Albania in its regional  
2 Eastern Mediterranean context, *Tectonophysics*, 316, 197-254, 2000.
- 3 Rolandi, G., Bellucci, F., Heizler, M. T., Belkin, H. E., and De Vivo, B.: Tectonic controls on  
4 the genesis of ignimbrites from the Campanian Volcanic Zone, southern Italy, *Miner. Petrol.*,  
5 79, 3-31, 2003.
- 6 Rotolo, S. G., Scaillet, S., La Felice, S., and Vita-Sceillet, G.: A revision of the structure and  
7 stratigraphy of pre-Green Tuff ignimbrites at Pantelleria (Strait of Sicily), *J. Volcanol. Geoth.  
8 Res.*, 250, 61-74, 2013.
- 9 Rouchon, V., Gillot, P. Y., Quidelleur, X., Chiesa, S., and Floris, B.: Temporal evolution of the  
10 Roccamonfina volcanic complex (Pleistocene), Central Italy, *J. Volcanol. Geoth. Res.*, 177,  
11 500-514, 2008.
- 12 Roulleau, E., Pinti, D. L., Rouchon, V., Quidelleur, X., and Gillot, P.-Y.: Tephro-  
13 chronostratigraphy of the lacustrine interglacial record of Piànico, Italian Southern Alps:  
14 Identifying the volcanic sources using radiogenic isotopes and trace elements, *Quatern. Int.*,  
15 204, 31-43, 2009.
- 16 Russo Ermolli, E., Aucelli, P. P. C., Di Rollo, A., Mattei, M., Petrosino, P., Porreca, M., and  
17 Rosskopf, C. M.: An integrated stratigraphical approach to the Middle Pleistocene succession  
18 of the Sessano basin (Molise, Italy), *Quatern. Int.*, 225, 114-127, 2010.
- 19 Sagnotti, L., Scardia, G., Giaccio, B., Liddicoat, J. C., Nomade, S., Renne, P. R., and Sprain,  
20 C. J.: Extremely rapid directional change during Matuyama-Brunhes geomagnetic polarity  
21 reversal, *Geophysical Journal International*, 199, 1110-1124, 2014.
- 22 Santacroce, R., Cioni, R., Marianelli, P., Sbrana, A., Sulpizio, R., Zanchetta, G., Donahue, D.  
23 J., and Joron, J. L.: Age and whole rock–glass compositions of proximal pyroclastics from the  
24 major explosive eruptions of Somma-Vesuvius: A review as a tool for distal tephrostratigraphy,  
25 *J. Volcanol. Geoth. Res.*, 177, 1-18, 2008.
- 26 Sarna-Wojcicki, A.: Tephrochronology, in: *Quaternary Geochronology*, edited by: Noller, J. S.,  
27 Sowers, J. M., and Lettis, W. R., AGU Reference Shelf, American Geophysical Union,  
28 Washington, DC, 2013.
- 29 Satow, C., Tomlinson, E. L., Grant, K. M., Albert, P. G., Smith, V. C., Manning, C. J., Ottolini,  
30 L., Wulf, S., Rohling, E. J., Lowe, J. J., Blockley, S. P. E., and Menzies, M. A.: A new  
31 contribution to the Late Quaternary tephrostratigraphy of the Mediterranean: Aegean Sea core  
32 LC21, *Quaternary Sci. Rev.*, 117, 96-112, 2015.
- 33 Scaillet, S., Vita-Sceillet, G., and Rotolo, S. G.: Millennial-scale phase relationships between  
34 ice-core and Mediterranean marine records: insights from high-precision  $^{40}\text{Ar}/^{39}\text{Ar}$  dating of  
35 the Green Tuff of Pantelleria, Sicily Strait, *Quaternary Sci. Rev.*, 78, 141-154, 2013.
- 36 Siani, G., Sulpizio, R., Paterne, M., and Sbrana, A.: Tephrostratigraphy study for the last 18,000  
37 C-14 years in a deep-sea sediment sequence for the South Adriatic, *Quaternary Sci Rev*, 23,  
38 2485-2500, 2004.
- 39 Sottilli, G., Palladino, D. M., and Zanon, V.: Plinian activity during the early eruptive history of  
40 the Sabatini volcanic district, central Italy, *J. Volcanol. Geoth. Res.*, 135, 361-379, 2004.
- 41 St. Seymour, K., Christanis, K., Bouzinos, A., Papazimou, S., Papatheodorou, G., Moran, E.,  
42 and Denes, G.: Tephrostratigraphy and tephrochronology in the Philippi peat basin, Macedonia,  
43 Northern Hellas (Greece), *Quatern. Int.*, 121, 53-65, 2004.

- 1 Steiger, R. H. and Jäger, E.: Subcommission on geochronology: Convention on the use of decay  
2 constants in geo- and cosmochronology, *Earth Planet. Sc.*, 36, 359-362, 1977.
- 3 Stoppa, F., Rosatelli, G., Wall, F., and Jeffries, T.: Geochemistry of carbonatite–silicate pairs  
4 in nature: A case history from Central Italy, *Lithos*, 85, 26-47, 2005.
- 5 Sulpizio, R., Zanchetta, G., Paterne, M., and Siani, G.: A review of tephrostratigraphy in central  
6 and southern Italy during the last 65 ka, *Il Quaternario Italiano J. Quaternary Sci.*, 16, 91-108,  
7 2003.
- 8 Sulpizio, R., Bonasia, R., Dellino, P., Di Vito, M. A., La Volpe, L., Mele, D., Zanchetta, G.,  
9 and Sadori, L.: Discriminating the long distance dispersal of fine ash from sustained columns  
10 or near ground ash clouds: The example of the Pomice di Avellino eruption (Somma-Vesuvius,  
11 Italy), *J. Volcanol. Geoth. Res.*, 177, 263-276, 2008.
- 12 Sulpizio, R., Zanchetta, G., D'Orazio, M., Vogel, H., and Wagner, B.: Tephrostratigraphy and  
13 tephrochronology of Lakes Ohrid and Prespa, Balkans, *Biogeosciences*, 7, 3273-3288, 2010.
- 14 Sulpizio, R., Alcicek, M. C., Zanchetta, G., and Solari, L.: Recognition of the Minoan tephra in  
15 the Acıgöl Basin, Western Turkey: implications for inter-archive correlations and fine ash  
16 dispersal, *J. Quaternary Sci.*, 28, 329-335, 2013.
- 17 Sumita, M. and Schmincke, H.-U.: Impact of volcanism on the evolution of Lake Van II:  
18 Temporal evolution of explosive volcanism of Nemrut Volcano (eastern Anatolia) during the  
19 past ca. 0.4 Ma, *J. Volcanol. Geoth. Res.*, 253, 15-34, 2013.
- 20 Tamburrino, S., Insinga, D. D., Sprovieri, M., Petrosino, P., and Tiepolo, M.: Major and trace  
21 element characterization of tephra layers offshore Pantelleria Island: insights into the last 200  
22 ka of volcanic activity and contribution to the Mediterranean tephrochronology, *J. Quaternary  
23 Sci.*, 27, 129-140, 2012.
- 24 Thunell, R., Federman, A., Sparks, S., and Williams, D.: Age, origin and volcanological  
25 significance of the Y-5 ash layer in the Mediterranean, *Quaternary Res.*, 12, 241-253, 1979.
- 26 Tomlinson, E. L., Arienzio, I., Civetta, L., Wulf, S., Smith, V. C., Hardiman, M., Lane, C. S.,  
27 Carandente, A., Orsi, G., Rosi, M., Müller, W., and Menzies, M. A.: Geochemistry of the  
28 Phlegraean Fields (Italy) proximal sources for major Mediterranean tephras: Implications for  
29 the dispersal of Plinian and co-ignimbritic components of explosive eruptions, *Geochim.  
30 Cosmochim. Ac.*, 93, 102-128, 2012.
- 31 Tomlinson, E. L., Smith, V. C., Albert, P. G., Aydar, E., Civetta, L., Cioni, R., Çubukçu, E.,  
32 Gertisser, R., Isaia, R., Menzies, M. A., Orsi, G., Rosi, M., and Zanchetta, G.: The major and  
33 trace element glass compositions of the productive Mediterranean volcanic sources: tools for  
34 correlating distal tephra layers in and around Europe, *Quaternary Sci. Rev.*, 118, 48-66, 2015.
- 35 Ton-That, T., Singer, B., and Paterne, M.: Ar-40/Ar-39 dating of latest Pleistocene (41 ka)  
36 marine tephra in the Mediterranean Sea: implications for global climate records, *Earth Planet.  
37 Sc.*, 184, 645-658, 2001.
- 38 Turbeville, B. N.: Tephra Fountaining, Rheomorphism, and Spatter Flow during Emplacement  
39 of the Pitigliano Tuffs, Latera-Caldera, Italy, *J. Volcanol. Geoth. Res.*, 53, 309-327, 1992a.
- 40 Turbeville, B. N.: 40Ar/39Ar Ages and stratigraphy of the Latera caldera, Italy, *B. Volcanol.*,  
41 55, 110-118, 1992b.
- 42 Tzedakis, P. C.: Long-term tree populations in northwest Greece through multiple Quaternary  
43 climatic cycles, *Nature*, 364, 437-440, 1993.

- 1 Vezzoli, L.: Tephra Layers in Bannock Basin (Eastern Mediterranean), Mar. Geol., 100, 21-34,  
2 1991.
- 3 Villa, I.M. and Buettner, A.: Chronostratigraphy of Monte Vulture volcano (southern Italy):  
4 secondary mineral microtextures and  $39\text{Ar}$ - $40\text{Ar}$  systematics. B. Volcanol., 71, 1195-1208,  
5 2009.
- 6 Vogel, H., Zanchetta, G., Sulpizio, R., Wagner, B., and Nowaczyk, N.: A tephrostratigraphic  
7 record for the last glacial-interglacial cycle from Lake Ohrid, Albania and Macedonia, J.  
8 Quaternary Sci., 25, 320-338, 2010.
- 9 Wagner, B., Reicherter, K., Daut, G., Wessels, M., Matzinger, A., Schwalb, A., Spirkovski, Z.,  
10 and Sanxhaku, M.: The potential of Lake Ohrid for long-term palaeoenvironmental  
11 reconstructions, Palaeogeography Palaeoclimatology Palaeoecology, 259, 341-356, 2008.
- 12 Wagner, B., Vogel, H., Zanchetta, G., and Sulpizio, R.: Environmental change within the  
13 Balkan region during the past ca. 50 ka recorded in the sediments from lakes Prespa and Ohrid,  
14 Biogeosciences, 7, 3187-3198, 2010.
- 15 Wagner, B., Francke, A., Sulpizio, R., Zanchetta, G., Lindhorst, K., Krastel, S., Vogel, H.,  
16 Rethemeyer, J., Daut, G., Grazhdani, A., Lushaj, B., and Trajanovski, S.: Possible earthquake  
17 trigger for 6th century mass wasting deposit at Lake Ohrid (Macedonia/Albania), Clim. Past, 8,  
18 2069-2078, 2012.
- 19 Wagner, B., Wilke, T., Krastel, S., Zanchetta, G., Sulpizio, R., Reicherter, K., Leng, M. J.,  
20 Grazhdani, A., Trajanovski, S., Francke, A., Lindhorst, K., Levkov, Z., Cvetkoska, A., Reed, J.  
21 M., Zhang, X., Lacey, J. H., Wonik, T., Baumgarten, H., and Vogel, H.: The SCOPSCO drilling  
22 project recovers more than 1.2 million years of history from Lake Ohrid, Scientific Drilling,  
23 17, 19-29, 2014.
- 24 Washington, H. S.: The Roman comagmatic region, Carnegie Institution of Washington, 1906.
- 25 Watzin, M. C., Puka, V., and Naumoski, T. B.: Lake Ohrid and Its Watershed: Our Lake, Our  
26 Future. A State of the Environment Report., Tirana, Albania and Ohrid, Macedonia, 134 pp.,  
27 2002.
- 28 Wulf, S., Kraml, M., Brauer, A., Keller, J., and Negendank, J. F. W.: Tephrochronology of the  
29 100ka lacustrine sediment record of Lago Grande di Monticchio (Southern Italy), Quatern. Int.,  
30 122, 7-30, 2004.
- 31 Wulf, S., Brauer, A., Mingram, J., Zolitschka, B., and Negendank, J. F. W.: Distal tephras in  
32 the sediments of Monticchio maar lakes, Principe, C., Regione Basilicata, Dipartimento  
33 Ambiente, Territorio e Politiche della Sostenibilità 2006.
- 34 Wulf, S., Keller, J., Paterne, M., Mingram, J., Lauterbach, S., Opitz, S., Sottili, G., Giaccio, B.,  
35 Albert, P. G., Satow, C., Tomlinson, E. L., Viccaro, M., and Brauer, A.: The 100–133 ka record  
36 of Italian explosive volcanism and revised tephrochronology of Lago Grande di Monticchio,  
37 Quaternary Sci. Rev., 58, 104-123, 2012.
- 38 Zanchetta, G., Sulpizio, R., Giaccio, B., Siani, G., Paterne, M., Wulf, S., and D'Orazio, M.: The  
39 Y-3 tephra: A Last Glacial stratigraphic marker for the Central Mediterranean Basin, J.  
40 Volcanol. Geoth. Res., 177, 145-154, 2008.
- 41 Zanchetta, G., Sulpizio, R., Roberts, N., Cioni, R., Eastwood, W. J., Siani, G., Caron, B.,  
42 Paterne, M., and Santacroce, R.: Tephrostratigraphy, chronology and climatic events of the  
43 Mediterranean basin during the Holocene: An overview, Holocene, 21, 33-52, 2011.

1 Zanchetta, G., Regattieri, E., Giaccio, B., Wagner, B., Sulpizio, R., Francke, A., Vogel, L. H.,  
2 Sadori, L., Masi, A., Sinopoli, G., Lacey, J. H., Leng, M. L., and Leicher, N.: Aligning MIS5  
3 proxy records from Lake Ohrid (FYROM) with independently dated Mediterranean archives:  
4 implications for core chronology, *Biogeosciences Discuss.*, 12, 16979-17007, 2015.

		SiO <sub>2</sub>	TiO <sub>2</sub>	Al <sub>2</sub> O <sub>3</sub>	FeO <sub>TOT</sub>	MnO	MgO	CaO	Na <sub>2</sub> O	K <sub>2</sub> O	P <sub>2</sub> O <sub>5</sub>	F	Cl	SO <sub>3</sub>	Total	Tot. Alkali	Alk. Ratio	
<b>OH-DP-0027</b>		̄x	56.29	0.11	23.80	1.44	0.08	0.33	1.55	8.69	7.21	-	-	0.50	-	100.00	15.90	0.83
n=12		s	0.51	0.09	0.18	0.16	0.09	0.18	0.11	0.35	0.20	-	-	0.12	-	-	0.28	0.05
OT0702-3		̄x	59.10	0.17	21.58	1.95	0.17	0.16	1.76	7.56	7.02	-	-	0.52	-	100.00	14.58	0.93
n=9		s	0.51	0.08	0.12	0.11	0.06	0.09	0.13	0.53	0.26	-	-	0.03	-	-	0.66	0.07
Co1262-709			58.59	0.17	21.81	1.84	0.16	0.12	1.67	8.20	6.94	0.00	-	0.51	-	100	15.14	0.85
n=12			0.39	0.08	0.49	0.12	0.06	0.08	0.22	0.50	0.29	0.00	-	0.03	-	-	0.36	0.08
PT0915-2		̄x	58.34	0.18	21.59	1.92	0.15	0.24	1.97	7.93	6.85	0.09	-	0.73	-	100.00	14.79	0.87
n=10		s	0.30	0.05	0.38	0.12	0.06	0.10	0.42	0.24	0.18	0.18	-	0.06	-	-	0.33	0.03
TM-6a		̄x	59.98	0.30	20.61	2.24	0.13	0.16	2.42	5.58	8.02	0.08	0.08	0.51	-	97.67	13.60	1.51
n=13		s	0.93	0.09	0.51	0.46	0.04	0.07	0.39	1.03	0.82	0.12	0.00	0.15	-	0.91	0.57	0.38
TM-6b		̄x	58.71	0.16	21.10	1.99	0.19	0.15	2.11	8.14	6.82	0.13	0.10	0.49	-	98.21	14.96	0.88
n=12		s	1.53	0.09	0.83	1.00	0.07	0.26	1.19	1.11	0.88	0.20	0.09	0.18	-	1.27	0.97	0.31
MJ1/VJ1		̄x	58.76	0.21	21.03	1.85	0.19	0.12	2.41	7.38	7.12	-	0.30	0.57	0.06	98.12	14.51	0.96
n=27		s	1.42	0.11	0.81	0.81	0.08	0.21	1.24	0.73	0.85	-	0.18	0.21	0.04	0.88	1.51	0.07
KET8218 V1		̄x	60.04	0.10	21.49	1.74	0.00	0.00	1.82	7.72	7.05	-	-			99.96	14.77	0.91
n=n.a.		s	-	-	-	-	-	-	-	-	-	-	-	-	-	-	-	-
IN68-9 125cm		̄x	59.50	0.09	21.26	1.71	0.11	0.14	1.81	7.72	7.14	-	-	0.52	-	93.40	93.40	0.92
n=20		s	0.78	0.02	0.34	0.17	0.06	0.12	0.43	0.57	0.62	-	-	0.08	-	3.53	3.53	0.11
IN68-5 259cm		̄x	58.81	0.09	21.21	1.79	0.12	0.10	1.75	8.18	7.40	-	-	0.55	-	95.54	15.58	0.91
n=15		s	0.36	0.03	0.15	0.10	0.06	0.07	0.09	0.37	0.13	-	-	0.04	-	1.82	0.33	0.05
RF95-11 320cm		̄x	59.10	0.11	20.60	1.89	0.13	0.08	1.88	7.58	8.13	-	-	0.50	-	95.94	15.71	1.08
n=21		s	0.76	0.05	0.26	0.30	0.06	0.05	0.36	0.67	0.45	-	-	0.12	-	1.64	0.84	0.11
RF95-11 320cm		̄x	61.43	0.27	18.46	2.95	0.12	0.32	1.97	5.29	8.52	-	-	0.67	-	94.95	13.81	1.65
n=3		s	0.56	0.06	0.09	0.24	0.07	0.28	0.19	0.83	0.94	-	-	0.21	-	1.18	0.40	0.24
MD90-918 210cm		̄x	58.71	0.14	21.82	1.78	0.17	0.17	1.74	8.06	6.80	-	-	0.60	-	-	14.86	0.85
n=9		s	0.47	0.08	0.23	0.11	0.10	0.06	0.16	0.35	0.15	-	-	0.11	-	-	0.38	0.04
MD90-918 223cm		̄x	58.82	0.12	21.88	1.72	0.13	0.11	1.81	8.27	6.60	-	-	0.53	-	100.00	14.88	0.80
n=12		s	0.61	0.10	0.28	0.15	0.12	0.06	0.53	0.37	0.81	-	-	0.09	-	-	1.00	0.10
AD94-17 190-191 cm		̄x	58.69	0.14	21.97	1.70	0.14	0.26	1.72	8.17	6.73	-	-	0.49	-	100.00	14.90	0.82
n=14		s	0.74	0.11	0.21	0.16	0.09	0.09	0.34	0.43	0.47	-	-	0.09	-	-	0.79	0.05
AD94-17 195-196cm		̄x	58.51	0.13	22.13	1.73	0.15	0.43	1.68	8.13	6.65	-	-	0.51	-	100.00	14.78	0.83
n=10		s	0.31	0.07	0.32	0.15	0.09	0.09	0.21	0.79	0.45	-	-	0.06	-	-	0.38	0.15
<b>OH-DP-0115</b>		̄x	61.60	0.38	18.24	3.43	0.12	0.70	2.67	3.43	9.32	0.10	0.14	0.46	0.11	95.49	12.76	2.77
n=16		s	0.89	0.03	0.17	0.32	0.05	0.16	0.32	0.44	0.44	0.04	0.09	0.10	0.06	1.98	0.15	0.45
OT0702-4		̄x	61.27	0.39	18.70	3.11	0.11	0.67	2.35	3.73	9.22	-	-	0.46	-	100.00	12.96	2.52
n=12		s	0.61	0.05	0.12	0.20	0.06	0.17	0.24	0.44	0.46	-	-	0.10	-	-	0.11	0.42
OT0520-2		̄x	61.88	0.29	18.63	2.92	0.03	0.50	2.20	4.18	8.82	-	-	0.54	-	100.00	12.99	2.15
n=12		s	0.50	0.08	0.18	0.22	0.06	0.15	0.18	0.45	0.49	-	-	0.13	-	-	0.09	0.35
JO187		̄x	60.99	0.40	18.74	3.26	0.11	0.68	2.38	3.59	9.43	-	-	0.42	-	100.00	13.02	2.68
n=10		s	0.71	0.10	0.10	0.26	0.07	0.15	0.25	0.48	0.41	-	-	0.09	-	-	0.28	0.46
OT0700-1		̄x	61.60	0.38	18.74	3.03	0.10	0.67	2.30	3.74	8.94	-	-	0.50	-	100.00	12.68	2.44
n=12		s	0.75	0.10	0.15	0.34	0.09	0.16	0.30	0.44	0.43	-	-	0.13	-	-	0.24	0.39
PT0915-5		̄x	60.85	0.40	18.92	3.40	0.11	0.79	2.37	3.60	8.94	0.01	-	0.62	-	100.00	12.54	2.57
n=12		s	0.87	0.08	0.27	0.37	0.07	0.19	0.30	0.58	0.56	0.03	-	0.19	-	-	0.27	0.56

			SiO <sub>2</sub>	TiO <sub>2</sub>	Al <sub>2</sub> O <sub>3</sub>	FeO <sub>TOT</sub>	MnO	MgO	CaO	Na <sub>2</sub> O	K <sub>2</sub> O	P <sub>2</sub> O <sub>5</sub>	F	Cl	SO <sub>3</sub>	Total*	Tot. Alkali	Alk. Ratio
M25/4-12	Y-3	̄	61.32	0.37	18.27	3.23	0.12	0.62	2.42	3.64	9.41	0.11	-	0.50	-	96.22	13.04	2.69
n=33		s	0.89	0.03	0.26	0.34	0.05	0.19	0.26	0.62	0.69	0.04	-	0.18	-	1.35	0.17	0.61
RC9 191	Y-3	̄	62.76	0.36	18.21	2.98	0.17	0.25	2.07	4.44	8.75	-	-	-	-	-	-	-
n=n.a.		s	0.36	0.03	0.16	0.21	0.12	0.12	0.15	0.19	0.26	-	-	-	-	-	-	-
TM-15		̄	62.22	0.38	18.36	3.27	0.13	0.61	2.19	3.85	8.36	0.12	-	0.52	-	96.32	12.21	2.21
n=20		s	0.76	0.03	0.20	0.29	0.04	0.14	0.22	0.43	0.54	0.06	-	0.10	-	0.46	0.21	0.36
TP-9.70		̄	61.79	0.37	18.28	3.17	0.10	0.59	2.40	3.78	9.19	0.12	-	0.54	-	96.46	12.97	2.48
n=42		s	0.78	0.04	0.17	0.31	0.04	0.14	0.22	0.47	0.47	0.04	-	0.12	-	1.42	0.19	0.41
S-19		̄	62.17	0.31	18.77	2.96	0.08	0.49	2.13	4.20	8.90	-	-	-	-	100.01	13.10	2.12
n=n.a.		s	1.15	0.07	0.14	0.47	0.04	0.26	0.29	0.38	0.50	-	-	-	-	-	-	-
C106 A2		̄	62.63	0.34	18.24	3.15	0.15	0.47	2.12	4.15	8.75	-	-	-	-	100.00	12.90	2.11
n=12		s	0.20	0.06	0.12	0.12	0.08	0.08	0.10	0.19	0.14	-	-	-	-	-	-	-
C45 B2		̄	62.41	0.33	18.30	3.17	0.15	0.50	2.13	4.30	8.71	-	-	-	-	100.00	13.01	2.03
n=11		s	0.32	0.10	0.29	0.10	0.08	0.09	0.10	0.15	0.08	-	-	-	-	-	-	-
MD90-917 920-17		̄	61.41	0.37	18.72	3.17	0.08	0.70	2.44	3.52	9.14	-	-	0.44	-	100.00	12.66	2.60
n=n.a.		s	0.86	0.10	0.17	0.38	0.08	0.21	0.33	0.40	0.40	-	-	0.09	-	-	-	-
KET8004	C-7	̄	63.12	0.25	18.53	3.03	0.00	0.14	2.17	3.86	8.86	-	-	-	-	99.96	12.72	2.30
n=n.a.		s	0.90	0.08	0.21	0.39	0.00	0.13	0.33	0.52	0.42	-	-	-	-	-	-	-
KET8011	C-7	̄	61.90	0.33	19.14	2.95	0.00	0.49	2.75	3.62	8.79	-	-	-	-	99.97	12.41	2.43
n=n.a.		s	-	-	-	-	-	-	-	-	-	-	-	-	-	-	-	-
<b>OH-DP-0169b</b>		̄	61.76	0.43	18.86	3.01	0.25	0.36	1.86	5.96	7.47	0.04	0.33	0.83	0.05	97.04	13.43	1.26
n=18		s	0.31	30.67	9.22	7.93	1.38	0.06	0.75	2.05	0.81	3.72	0.15	0.26	0.39	1.25	0.31	0.07
<b>OH-DP-0169a</b>		̄	61.69	0.41	18.89	3.04	0.26	0.34	1.78	6.28	7.28	0.04	0.36	0.85	0.05	98.78	13.56	1.17
n=25		s	0.44	0.03	0.14	0.09	0.04	0.02	0.04	0.56	0.15	0.02	0.07	0.04	0.02	1.56	0.57	0.17
OT0700-2		̄	60.84	0.39	19.21	2.98	0.20	0.42	1.77	6.06	7.45	-	-	0.68	-	100.00	13.51	1.29
n=17		s	0.38	0.09	0.18	0.19	0.07	0.12	0.25	0.82	0.72	-	-	0.11	-	-	0.33	0.50
OT05020-3		̄	61.88	0.29	18.63	2.92	0.03	0.50	2.20	4.18	8.82	-	-	0.54	-	100.00	12.99	2.15
n=12		s	0.50	0.08	0.18	0.22	0.06	0.15	0.18	0.45	0.49	-	-	0.13	-	-	0.09	0.37
OT0702-6		̄	60.83	0.40	19.13	2.93	0.18	0.48	1.77	6.31	7.34	-	-	0.65	-	100.00	13.65	1.17
n=11		s	0.30	0.10	0.11	0.13	0.09	0.08	0.20	0.44	0.25	-	-	0.10	-	-	0.31	0.13
JO-244		̄	60.64	0.42	19.18	2.96	0.21	0.40	1.81	6.22	7.48	-	-	0.69	-	100.00	13.69	1.21
n=18		s	0.57	0.08	0.24	0.16	0.05	0.12	0.21	0.36	0.31	-	-	0.10	-	-	0.20	0.13
OT0701-1/5		̄	60.92	0.41	19.15	3.02	0.20	0.44	1.80	5.87	7.57	-	-	0.64	-	100.00	13.44	1.37
n=41		s	0.64	0.07	0.69	0.18	0.07	0.14	0.30	1.12	0.97	-	-	0.14	-	-	0.38	0.69
PT0704-3		̄	60.83	0.42	19.14	3.03	0.23	0.47	1.77	5.86	7.59	-	-	0.65	-	100.00	13.46	1.53
n=105		s	0.58	0.09	0.23	0.26	0.09	0.16	0.32	1.01	0.82	-	-	0.13	-	-	0.42	0.69
RC9 191 Y-5		̄	61.56	0.44	18.90	3.59	0.17	0.59	1.97	5.55	7.26	-	-	-	-	96.48	12.80	1.31
V10 58 Y-5		s	62.46	0.36	18.43	2.11	0.16	0.40	2.16	6.33	7.59	-	-	-	-	93.52	13.92	1.20
C-13		̄	62.20	0.35	19.30	2.94	0.08	1.75	5.92	7.41	-	-	-	-	-	99.95	13.33	1.25
C-13		s	61.50	0.31	19.15	3.13	0.33	2.50	3.54	9.50	-	-	-	-	-	99.96	13.04	2.68
PRAD 1653		̄	61.00	0.43	19.71	2.93	0.24	0.28	1.68	6.72	7.01	-	-	-	-	95.89	13.73	1.04
n=14		s	0.49	0.04	0.11	0.29	0.04	0.03	0.07	0.20	0.12	-	-	-	-	0.87	0.27	0.03
I-3		̄	61.45	0.41	18.40	3.12	0.19	0.54	2.16	4.88	7.84	0.09	0.26	0.65	-	97.01	12.84	1.72
n=14		s	1.14	0.05	0.43	0.43	0.06	0.24	0.56	0.94	0.97	0.06	0.11	0.21	-	2.48	0.47	0.63
Lc 21 4.925		̄	61.93	0.46	18.03	3.20	0.21	0.44	2.05	6.20	7.46	-	-	-	-	95.35	13.66	1.25
n=32		s	0.74	0.10	0.25	0.47	0.08	0.36	0.70	0.94	0.48	-	-	-	-	1.33	0.93	0.30

		SiO <sub>2</sub>	TiO <sub>2</sub>	Al <sub>2</sub> O <sub>3</sub>	FeO <sub>TOT</sub>	MnO	MgO	CaO	Na <sub>2</sub> O	K <sub>2</sub> O	P <sub>2</sub> O <sub>5</sub>	F	Cl	SO <sub>3</sub>	Total*	Tot. Alkali	Alk. Ratio	
TM18		̄x	61.60	0.43	18.92	2.93	0.24	0.35	1.75	5.78	7.04	0.05	0.33	0.79	-	98.64	12.82	1.24
n=61		s	0.46	0.03	0.36	0.11	0.03	0.07	0.16	0.75	0.53	0.02	0.04	0.08	-	1.71	0.83	0.25
ML2		̄x	61.01	0.48	18.18	3.02	0.21	0.44	2.12	5.64	8.05	-	0.07	0.71	-	96.51	13.70	1.57
n=105		s	0.42	0.04	0.19	0.21	0.06	0.15	0.32	1.20	1.02	-	0.04	0.20	-	1.46	0.32	0.69
S-17		̄x	61.67	0.33	19.18	2.90	0.22	0.27	1.60	6.42	7.38	-	-	-	-	100.00	13.80	1.15
n=n.a.		s	0.22	0.14	0.10	0.10	0.10	0.08	0.11	0.30	0.20	-	-	-	-	-	0.50	-
Tenaghi Phlippon CI		̄x	63.29	0.40	19.42	3.32	0.20	0.45	2.09	5.20	8.48	0.10	-	-	-	96.42	13.69	1.99
n=3		s	0.39	0.03	0.28	0.26	0.06	0.20	0.47	1.69	1.27	0.06	-	-	-	0.88	0.46	1.13
pre CI deposits		̄x	58.94	0.40	19.75	3.45	0.25	0.34	2.04	6.46	7.58	-	-	0.79	-	97.76	14.04	1.19
n=68		s	0.38	0.02	0.16	0.14	0.03	0.04	0.10	0.51	0.30	-	-	0.04	-	1.32	0.26	0.14
<b>OH-DP-0404</b>		̄x	57.49	0.54	19.05	5.10	0.17	1.30	4.33	4.06	7.72	0.24	0.18	0.50	0.09	97.08	11.78	1.93
n=20		s	1.00	0.11	0.45	0.67	0.04	0.24	0.65	0.54	0.62	0.07	0.08	0.09	0.05	1.33	0.93	0.25
OT0702-8		̄x	57.60	0.55	19.49	4.48	0.16	1.22	3.77	4.18	8.09	0.01	-	0.46	-	100.00	12.26	1.94
n=12		s	0.46	0.08	0.15	0.33	0.07	0.15	0.32	0.18	0.43	0.02	-	0.05	-	-	0.43	0.15
TM-24a		̄x	57.64	0.49	18.99	4.26	0.14	1.12	3.99	4.24	8.37	0.24	-	0.52	-	100.00	12.61	1.97
n=35		s	1.14	0.06	0.19	0.46	0.02	0.22	0.56	0.14	0.31	0.06	-	0.04	-	0.01	0.31	0.11
POP2		̄x	59.71	0.42	18.43	3.79	0.17	0.73	2.94	4.26	8.61	0.09	0.14	0.54	0.15	96.28	12.87	2.02
n=26		s	1.10	0.07	0.11	0.62	0.05	0.25	0.57	0.17	0.34	0.05	0.07	0.06	0.06	1.34	0.48	0.07
RF93-77 797cm		̄x	59.41	0.41	19.17	3.69	0.10	0.77	2.84	4.36	8.75	-	-	0.50	-	97.24	13.11	2.01
n=n.a.		s	0.41	0.08	0.10	0.18	0.07	0.15	0.20	0.36	0.30	-	-	0.07	-	0.81	0.66	-
CM92-42 710cm		̄x	59.19	0.41	19.20	3.74	0.08	0.81	2.99	4.25	8.84	-	-	0.49	-	97.65	13.09	2.08
n=n.a.		s	0.39	0.07	0.17	0.22	0.05	0.11	0.22	0.30	0.23	-	-	0.07	-	1.46	0.53	-
<b>OH-DP-0435</b>		̄x	61.06	0.45	18.53	3.09	0.30	0.36	1.78	6.12	6.98	0.05	0.37	0.86	0.05	96.82	13.10	1.16
n=22		s	0.34	0.04	0.17	0.12	0.10	0.09	0.10	0.52	0.55	0.03	0.13	0.14	0.03	1.60	0.26	0.20
OT0702-9		̄x	61.15	0.46	18.82	3.09	0.29	0.39	1.68	6.39	7.03	-	-	0.71	-	100.00	13.42	1.12
n=15		s	0.30	0.06	0.12	0.14	0.09	0.10	0.08	0.62	0.50	-	-	0.14	-	-	0.20	0.20
JO575		̄x	61.20	0.47	18.74	2.97	0.29	0.38	1.65	6.54	7.04	-	-	0.72	-	100.00	13.58	1.09
n=20		s	0.43	0.08	0.17	0.15	0.08	0.08	0.11	0.61	0.45	-	-	0.12	-	-	0.32	0.17
22M-60 X-6		̄x	61.45	0.49	18.52	3.80	0.22	0.59	2.06	6.20	6.66	-	-	-	-	94.53	12.86	1.08
n=n.a.		s	-	-	-	-	-	-	-	-	-	-	-	-	-	-	-	-
TM27		̄x	61.43	0.46	18.57	2.85	0.23	0.40	1.84	6.32	7.25	0.06	-	0.71	-	97.86	13.57	1.17
n=22		s	0.40	0.02	0.09	0.13	0.06	0.08	0.11	0.66	0.50	0.04	-	0.14	-	1.40	0.24	0.19
POP4		̄x	61.49	0.45	18.26	3.08	0.25	0.38	1.77	5.84	7.36	0.04	0.28	0.75	0.05	97.05	13.20	1.28
n=31		s	0.42	0.03	0.11	0.11	0.07	0.06	0.08	0.52	0.43	0.02	0.10	0.14	0.03	1.31	0.28	0.17
S-10		̄x	62.38	0.40	18.86	2.81	0.24	0.29	1.61	6.02	7.39	-	-	-	-	-	13.41	1.23
n=n.a.		s	-	-	-	-	-	-	-	-	-	-	-	-	-	-	-	-
I-9		̄x	62.00	0.46	18.50	2.99	0.27	0.38	1.71	5.74	6.77	0.06	0.32	0.80	-	96.42	12.51	1.19
n=15		s	0.39	0.05	0.24	0.09	0.05	0.04	0.07	0.31	0.30	0.04	0.13	0.10	-	0.83	0.22	0.11
KET8004		̄x	61.80	0.45	18.11	3.16	0.28	0.31	1.76	5.64	7.34	0.02	0.14	1.00	-	-	12.98	1.30
DED8708 C-31		s	0.50	0.09	0.19	0.17	0.11	0.16	0.21	0.54	0.60	0.03	0.08	0.25	-	-	1.14	-
KET8282 C-31		̄x	61.74	0.49	19.19	3.10	-	0.43	1.72	6.03	7.31	-	-	-	-	-	13.34	1.21
n=n.a.		s	0.34	0.08	0.11	0.18	-	0.08	0.14	0.71	0.68	-	-	-	-	-	1.39	-

		SiO <sub>2</sub>	TiO <sub>2</sub>	Al <sub>2</sub> O <sub>3</sub>	FeO <sub>TOT</sub>	MnO	MgO	CaO	Na <sub>2</sub> O	K <sub>2</sub> O	P <sub>2</sub> O <sub>5</sub>	F	Cl	SO <sub>3</sub>	Total*	Tot. Alkali	Alk. Ratio
KET8222 C-31		60.17	0.47	19.45	3.70	-	0.77	2.51	4.03	8.69	-	-	-	-	-	12.72	2.16
n=n.a.	s	0.12	0.04	0.04	0.20	-	0.06	0.25	0.55	0.62	-	-	-	-	-	1.17	-
PRAD2812		62.00	0.46	18.84	2.93	0.24	0.39	1.75	6.10	7.29	-	-	-	-	96.21	13.39	1.22
n=23	s	0.24	0.03	0.10	0.11	0.07	0.08	0.08	0.62	0.55	-	-	-	-	0.85	0.15	0.21
C1202 t1		60.16	0.45	18.36	3.30	0.32	0.31	1.77	7.34	6.60	0.17	0.30	0.91	-	96.82	13.94	1.05
n=20	s	0.28	0.12	0.25	0.22	0.11	0.08	0.11	0.21	0.21	0.12	0.18	0.06	-	1.81	0.26	0.03
CIL2		61.46	0.45	18.37	3.24	0.29	0.45	1.86	5.47	7.19	0.08	0.38	0.72	0.03	96.08	12.66	1.40
n=74	s	0.67	0.05	0.34	0.25	0.09	0.19	0.28	0.97	0.97	0.06	0.20	0.23	0.04	1.51	0.42	0.47
SM1		62.27	0.45	18.19	3.31	0.35	0.35	1.76	5.05	7.82	-	-	0.45	-	95.27	12.87	1.55
n=15	s	0.33	0.04	0.25	0.16	0.01	0.14	0.06	0.18	0.35	-	-	0.07	-	-	-	-
SM2		62.50	0.43	18.37	3.23	0.36	0.40	1.73	5.36	7.31	-	-	0.33	-	96.18	12.66	1.36
n=11	s	0.90	0.02	0.18	0.24	0.14	0.20	0.22	0.23	0.50	-	-	0.11	-	-	-	-
SA		62.21	0.41	18.50	3.34	0.22	0.42	1.80	4.77	7.94	-	-	0.39	-	96.36	12.71	1.66
n=16	s	0.24	0.07	0.17	0.09	0.10	0.07	0.09	0.21	0.16	-	-	0.10	-	-	-	-
<b>OH-DP-0499</b>		65.32	0.69	15.32	6.02	0.28	0.33	1.32	5.68	4.92	0.11	0.08	0.15	0.06	97.13	10.61	0.87
n=11 (trachyte)	s	1.06	0.08	0.88	0.31	0.04	0.09	0.25	0.36	0.09	0.04	0.05	0.05	0.02	1.70	0.41	0.05
<b>OH-DP-0499</b>		73.61	0.36	8.77	7.30	0.34	0.08	0.33	4.72	4.46	0.02	0.29	0.85	0.06	93.33	9.18	0.95
n=32 (pantellerite)	s	0.34	0.03	0.21	0.15	0.05	0.02	0.03	0.28	0.09	0.02	0.09	0.07	0.03	1.16	0.28	0.06
LC21 10.345		73.91	0.39	8.65	7.06	0.30	0.03	0.29	5.01	4.36	-	-	-	-	100.00	9.37	1.06
n=5	s	1.62	0.04	0.15	0.24	0.06	0.02	0.02	1.89	0.08	-	-	-	-	-	1.83	0.49
ODP3		65.05	0.75	15.61	5.66	0.29	0.41	1.43	5.85	4.78	0.15	0.07	0.10	-	96.81	10.64	0.95
n=14 (trachyte)	s	0.33	0.04	0.20	0.16	0.04	0.03	0.07	0.31	0.15	0.02	0.04	0.02	-	1.39	0.30	0.06
ODP3		73.58	0.39	9.40	6.63	0.32	0.10	0.31	4.83	4.43	0.02	0.24	0.68	-	94.78	9.25	1.40
n=4 (pantellerite)	s	0.98	0.02	1.21	0.83	0.02	0.05	0.01	0.61	0.11	0.01	0.08	0.17	-	2.21	0.64	0.10
TII5		75.46	0.38	8.99	7.28	0.22	0.06	0.30	6.24	4.59	-	-	-	-	95.94	10.82	0.74
n=15	s	0.57	0.04	0.14	0.28	0.09	0.02	0.03	0.30	0.26	-	-	-	-	0.69	0.31	0.85
ML5		66.22	0.75	14.33	6.05	0.30	0.27	1.16	5.59	4.99	-	-	-	-	95.86	10.58	0.90
n=6 (trachyte)	s	0.93	0.06	0.98	0.43	0.02	0.09	0.24	0.25	0.12	-	-	-	-	1.33	0.15	0.06
ML5		73.73	0.43	8.31	7.14	0.32	0.08	0.31	4.30	4.44	-	-	-	-	92.72	8.74	1.04
n=50 (pantellerite)	s	0.24	0.01	0.10	0.16	0.02	0.01	0.01	0.24	0.08	-	-	-	-	0.45	0.24	0.07
OT0702-10		66.18	0.43	16.23	5.96	0.23	0.20	0.84	5.85	5.79	-	0.13	-	-	100.00	11.64	0.99
n=3 (trachyte)	s	0.73	0.13	2.54	0.08	0.16	0.17	0.10	0.64	1.14	-	0.09	-	-	-	1.44	0.18
OT0702-10		72.52	0.41	9.34	6.70	0.31	0.12	0.34	5.06	4.50	-	0.71	-	-	100.00	9.55	0.91
n=6 (pantellerite)	s	0.72	0.08	1.12	0.36	0.05	0.06	0.06	0.64	0.28	-	0.07	-	-	-	0.56	0.17
JO941		72.28	0.37	8.54	6.79	0.29	0.10	0.29	6.33	4.39	-	0.69	-	-	100.00	10.71	0.69
n=13	s	0.26	0.11	0.09	0.10	0.09	0.21	0.05	0.18	0.09	-	0.05	-	-	-	0.14	0.48
KET8222 P-11		64.67	0.83	15.50	5.88	0.28	1.45	6.41	4.98	-	-	-	-	-	-	11.39	0.78
n=n.a. (trachyte)	s	0.68	0.10	0.71	0.19	0.14	0.20	0.27	0.19	-	-	-	-	-	-	0.46	-
KET8222 P-11		72.41	0.34	8.95	7.43	0.08	0.17	6.09	4.54	-	-	-	-	-	-	10.63	0.75
n=n.a. (pantellerite)	s	0.38	0.08	0.09	24.00	6.00	0.08	0.33	0.00	-	-	-	-	-	-	0.33	-
ODP2		63.92	1.00	16.22	5.35	0.25	0.99	2.50	5.55	3.89	0.35	0.09	0.24	-	97.22	9.44	0.82
n=18		1.74	0.30	0.83	0.51	0.04	0.61	1.18	0.43	0.80	0.37	0.07	0.11	-	1.18	0.87	0.10
ODP4		65.10	0.72	15.89	5.72	0.30	0.38	1.41	5.62	4.72	0.14	0.05	0.15	-	96.33	10.35	0.90
n=33 (trachyte)		0.61	0.04	0.47	0.14	0.04	0.08	0.12	0.38	0.12	0.04	0.05	0.23	-	1.55	0.39	0.06
ODP4		74.58	0.40	8.70	6.98	0.36	0.07	0.29	4.25	4.33	0.03	0.30	0.73	-	93.45	8.55	1.35
n=33 (pantellerite)		0.18	0.02	0.00	0.04	0.06	0.01	0.01	0.26	0.09	0.02	0.01	0.04	-	0.39	0.22	0.05

		SiO <sub>2</sub>	TiO <sub>2</sub>	Al <sub>2</sub> O <sub>3</sub>	FeO <sub>TOT</sub>	MnO	MgO	CaO	Na <sub>2</sub> O	K <sub>2</sub> O	P <sub>2</sub> O <sub>5</sub>	F	Cl	SO <sub>3</sub>	Total*	Tot. Alkali	Alk. Ratio	
<b>OH-DP-0617</b>		̄	60.15	0.43	19.77	2.75	0.15	0.42	2.38	5.04	8.85	0.05	0.49	0.24	0.12	94.36	13.89	1.76
n=13		s	0.33	0.02	0.28	0.09	0.04	0.02	0.06	0.16	0.26	0.02	0.10	0.02	0.04	1.62	0.16	0.10
CF5 V4		̄	58.90	0.48	20.46	3.20	0.18	0.62	2.71	5.00	8.37	0.08	0.47	0.25	0.11	95.85	13.37	1.68
n=16		s	1.81	0.10	0.22	1.03	0.03	0.48	0.98	0.37	0.39	0.10	0.15	0.07	0.04	0.81	0.73	0.08
OT0701-6		̄	59.58	0.44	20.04	2.76	0.13	0.51	2.31	5.24	8.80	-	-	0.18	-	100.00	14.04	1.68
n=15		s	0.22	0.07	0.12	0.14	0.09	0.08	0.09	0.15	0.16	-	-	0.04	-	-	0.10	0.08
Vico B		̄	59.66	0.46	19.59	2.85	0.15	0.42	2.37	5.37	8.65	0.05	0.43	0.22	0.09	95.32	14.02	1.61
n=13		s	0.26	0.07	0.10	0.05	0.04	0.03	0.05	0.09	0.16	0.04	0.11	0.02	0.03	1.31	0.14	0.05
<b>OH-DP-0624</b>		̄	51.40	1.02	18.17	8.00	0.19	3.09	8.36	3.20	5.88	0.68	0.19	0.34	0.37	97.77	9.08	1.84
n=19		s	3.60	0.22	0.62	2.13	0.03	1.17	2.48	0.68	1.45	0.28	0.06	0.08	0.17	1.29	2.08	0.18
OT0701-7		̄	55.79	0.81	19.24	5.30	0.18	1.67	5.14	4.20	7.19	0.16	-	0.37	-	100.00	11.40	1.73
n=22		s	3.92	0.28	0.63	2.49	0.08	1.25	2.67	0.71	1.58	0.16	-	0.07	-	-	2.27	0.13
PRAD3225		̄	57.82	0.68	19.12	4.15	0.19	1.05	4.05	4.88	8.08	-	-	-	-	97.21	12.95	1.65
n=11		s	2.77	0.16	0.39	1.73	0.01	0.90	2.00	0.60	1.10	-	-	-	-	1.19	1.68	0.06
CF5 V5		̄	54.92	0.81	18.76	6.08	0.19	1.98	5.93	3.82	7.06	0.46	0.21	0.41	0.24	96.59	10.88	1.86
n=14		s	3.56	0.22	0.58	2.12	0.05	1.06	2.09	0.64	1.12	0.30	0.08	0.08	0.08	1.39	1.71	0.13
C-42		̄	49.74	1.49	18.06	8.63	0.27	3.26	8.25	3.37	5.97	0.79	0.17	-	-	99.56	9.34	1.77
n=n.a.		s	1.08	0.30	0.26	0.61	0.17	0.21	0.56	0.13	0.24	0.19	0.05	-	-	-	0.37	-
Pittigliano tuff WDS		̄	58.89	0.60	19.65	3.42	-	0.15	0.78	3.69	4.16	8.59	0.08	0.21	-	98.41	12.75	2.09
n=3		s	1.71	0.11	0.37	1.36	-	0.01	0.66	1.58	0.50	1.56	0.00	0.13	-	0.61	1.65	0.48
Pittigliano tuff XRF		̄	58.69	0.57	19.43	1.74	1.96	0.15	0.71	3.25	4.03	9.28	0.12	0.00	0.00	96.51	13.32	2.38
n=3		s	1.33	0.05	0.19	0.36	0.39	0.00	0.30	0.87	0.59	1.04	0.09	0.00	0.00	0.61	0.80	0.56
<b>OH-DP-1817</b>		̄	44.48	0.98	15.44	10.76	0.23	4.61	13.25	3.81	5.48	0.95	0.36	0.14	0.41	97.58	9.28	1.47
n=10		s	1.60	0.12	0.97	1.02	0.06	0.44	1.40	0.59	0.47	0.13	0.11	0.02	0.18	0.85	0.77	0.24
AH20-Pra		̄	40.41	1.33	12.14	6.19	0.26	14.77	11.21	3.38	4.83	1.08	0.59	-	0.08	96.94	8.21	1.43
n=6		s	0.16	0.04	0.05	0.17	0.03	0.30	0.13	0.08	0.36	0.12	0.11	-	0.02	-	0.44	-
Sulmona Site 2		̄	41.92	1.19	14.23	12.50	0.32	5.20	14.20	4.00	5.43	1.02	0.49	0.16	0.16	96.95	9.43	1.37
n=23		s	0.63	0.05	0.19	0.35	0.03	0.18	0.37	0.31	0.28	0.08	0.08	0.02	0.05	1.38	0.32	0.15
Sulmona Site 2a		̄	43.01	1.17	14.77	11.53	0.28	4.75	13.59	3.83	6.07	1.00	0.45	0.14	0.14	97.61	9.90	1.64
n=30		s	1.40	0.15	0.94	1.16	0.06	1.01	1.57	0.41	1.46	0.13	0.12	0.02	0.07	1.12	1.21	0.60
Paganica site 5		̄	43.47	1.10	15.34	10.87	0.29	4.78	13.15	3.75	6.42	0.82	0.45	0.14	0.27	96.70	10.17	1.80
n=18		s	1.86	0.16	1.76	1.20	0.07	1.19	2.17	0.98	1.32	0.17	0.16	0.05	0.12	1.22	1.70	0.54
Raiano site 3		̄	43.68	1.06	14.49	10.62	0.27	5.24	13.69	3.53	6.53	0.88	0.44	0.13	0.21	97.79	10.06	1.85
n=22		s	1.04	0.21	1.42	0.76	0.05	1.06	1.55	0.31	1.20	0.13	0.11	0.02	0.14	0.66	1.30	0.34
PR basal fallout		̄	42.83	1.41	12.65	11.60	0.22	6.51	16.30	2.96	4.42	1.10	0.48	-	0.03	97.96	7.38	1.49
n=10		s	0.17	0.11	0.11	0.09	0.04	0.10	0.29	0.06	0.11	0.06	0.14	-	0.03	0.86	0.14	0.04
CF7-V11		̄	43.49	1.03	14.81	10.83	0.26	4.58	13.15	4.23	6.67	0.94	0.38	0.14	0.30	99.04	99.04	10.90
n=11		s	1.35	0.12	0.98	1.12	0.05	0.57	1.64	0.44	1.16	0.11	0.11	0.02	0.12	0.62	0.62	1.24

		SiO <sub>2</sub>	TiO <sub>2</sub>	Al <sub>2</sub> O <sub>3</sub>	FeO <sub>TOT</sub>	MnO	MgO	CaO	Na <sub>2</sub> O	K <sub>2</sub> O	P <sub>2</sub> O <sub>5</sub>	F	Cl	SO <sub>3</sub>	Total*	Tot. Alkali	Alk. Ratio	
<b>OH-DP-1955</b>		̄x	57.53	0.57	20.51	4.03	0.18	0.56	4.55	4.78	6.97	0.09	0.31	0.23	0.21	96.70	11.75	1.47
n=18		s	1.49	0.10	0.47	0.34	0.04	0.07	0.52	0.72	1.55	0.02	0.11	0.05	0.05	1.83	1.90	0.33
SC5		̄x	58.42	0.48	21.16	3.01	0.20	0.36	4.41	4.84	6.63	0.14	0.33	0.24	0.18	94.64	11.47	1.38
n=17		s	1.37	0.09	0.98	0.74	0.08	0.16	0.52	0.52	0.69	0.10	0.18	0.10	0.14	1.55	0.91	0.20
Fall B		̄x	60.09	0.48	19.06	2.92	0.16	0.50	3.26	3.14	10.34	0.05	-	-	-	100.00	13.48	3.78
n=6		s	0.25	0.01	0.09	0.08	0.02	0.04	0.17	0.15	0.12	0.01	-	-	-	-	0.25	0.16
<b>OH-DP-2010</b>		54.03	0.76	18.14	6.33	0.15	1.77	6.23	3.08	8.66	0.35	0.32	0.08	0.49	97.59	11.73	2.87	
n=22		3.62	0.17	0.72	1.75	0.03	0.81	1.81	0.49	0.89	0.19	0.11	0.03	0.16	1.77	1.10	0.43	
Fall A		59.92	0.50	19.21	3.16	0.17	0.51	3.19	3.05	10.20	0.08	-	-	-	100.00	13.25	3.36	
n=11		0.29	0.02	0.14	0.12	0.11	0.05	0.25	0.17	0.17	0.03	-	-	-	-	0.26	0.20	
SC3		58.47	0.54	18.80	3.85	0.15	0.91	3.93	2.89	9.75	0.09	0.30	0.07	0.26	96.81	12.64	3.40	
n=20		1.31	0.04	0.18	0.72	0.03	0.33	0.78	0.25	0.61	0.04	0.12	0.02	0.13	1.33	0.73	0.29	
A9		58.87	0.55	19.13	3.60	0.12	0.59	3.57	3.65	9.81	0.11	0.28	0.14	-	97.10	13.46	2.73	
n=16		1.13	0.24	0.37	0.73	0.10	0.22	0.69	0.38	0.60	0.11	0.14	0.07	-	1.25	0.38	0.41	
Sulmona 5-1c		60.13	0.44	19.05	3.01	0.14	0.55	3.16	3.09	10.33	0.06	0.00	0.11	0.38	95.15	13.42	3.36	
n=30		0.89	0.04	0.43	0.32	0.04	0.14	0.38	0.21	0.21	0.03	0.00	0.02	0.12	1.24	0.26	0.26	
FIC-12.9		55.52	0.63	19.41	4.75	0.19	1.28	5.34	4.38	8.27	0.23	0.43	0.11	0.31	96.51	12.65	1.95	
n=22		1.79	0.08	0.35	0.73	0.05	0.36	0.98	0.53	1.05	0.08	0.11	0.02	0.11	1.77	0.66	0.52	
<b>OH-DP-2017</b>		64.43	0.44	18.27	2.59	0.18	0.29	1.06	5.65	6.32	0.05	0.24	0.36	0.11	94.22	11.97	0.29	
n=21		0.20	0.08	0.12	0.08	0.03	0.02	0.05	0.26	0.14	0.03	0.07	0.02	0.03	0.60	1.12	0.06	
A11		63.68	0.46	18.28	2.73	0.18	0.42	1.44	5.17	7.13	0.15	0.11	0.24	-	96.52	12.30	1.41	
n=18		0.66	0.10	0.33	0.27	0.16	0.17	0.28	0.66	0.40	0.11	0.14	0.09	-	0.84	0.48	0.27	
A12		64.18	0.51	17.85	2.56	0.23	0.30	1.09	6.09	6.57	0.12	0.11	0.39	-	96.37	12.66	1.08	
n=17		0.53	0.12	0.23	0.23	0.16	0.09	0.20	0.33	0.20	0.12	0.13	0.08	-	0.92	0.31	0.08	
SC2		66.20	0.35	16.97	3.01	0.26	0.32	0.98	5.27	5.71	0.02	0.02	0.50	0.40	95.38	10.98	1.09	
n=16		0.58	0.03	0.17	0.21	0.03	0.13	0.26	0.27	0.12	0.02	0.01	0.04	0.10	1.21	0.32	0.05	
<b>OH-DP-2060</b>		44.94	0.78	18.67	8.44	0.29	1.61	10.91	5.39	7.74	0.28	0.91	0.19	0.95	96.34	13.13	1.46	
n=19		1.70	0.17	0.94	1.18	0.05	0.98	1.26	0.76	1.32	0.16	0.23	0.04	0.48	1.81	1.68	0.27	
SUL 1-6		44.73	0.82	19.48	8.17	0.36	1.45	10.90	5.59	8.31	0.18	0.85	0.18	0.75	96.73	13.90	1.53	
n=27		1.16	0.10	0.70	0.77	0.05	0.14	1.16	0.64	0.90	0.03	0.20	0.03	0.27	1.31	0.67	0.40	
Oricola tuff		45.15	0.00	18.83	8.27	0.32	1.52	11.40	4.90	8.33	0.23	0.79	0.13	0.13	100.00	13.23	1.70	
n=8		0.66	0.00	0.31	0.45	0.03	0.11	0.62	0.25	0.67	0.04	0.09	0.02	0.05	-	0.76	0.15	
proximal TBA		45.74	0.76	19.16	7.80	0.30	1.40	10.20	5.49	8.93	0.21	0.86	-	0.85	98.02	14.42	1.63	
n=7		0.79	0.11	0.14	0.19	0.03	0.06	0.46	0.27	0.29	0.03	0.14	-	0.10	0.70	0.27	0.12	

#### WDS standard

##### Standard 1 -

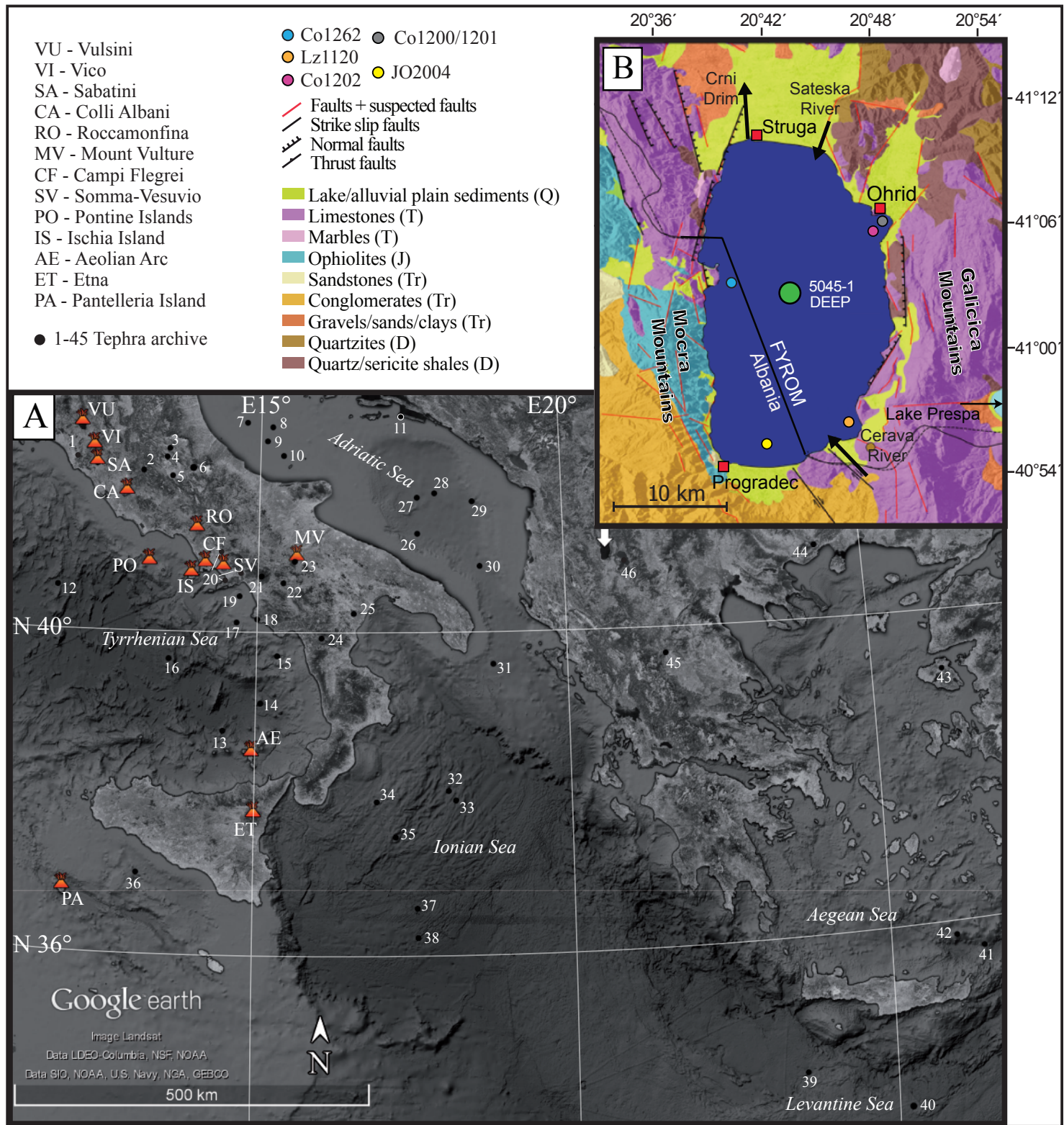
##### USGS Rhyolite

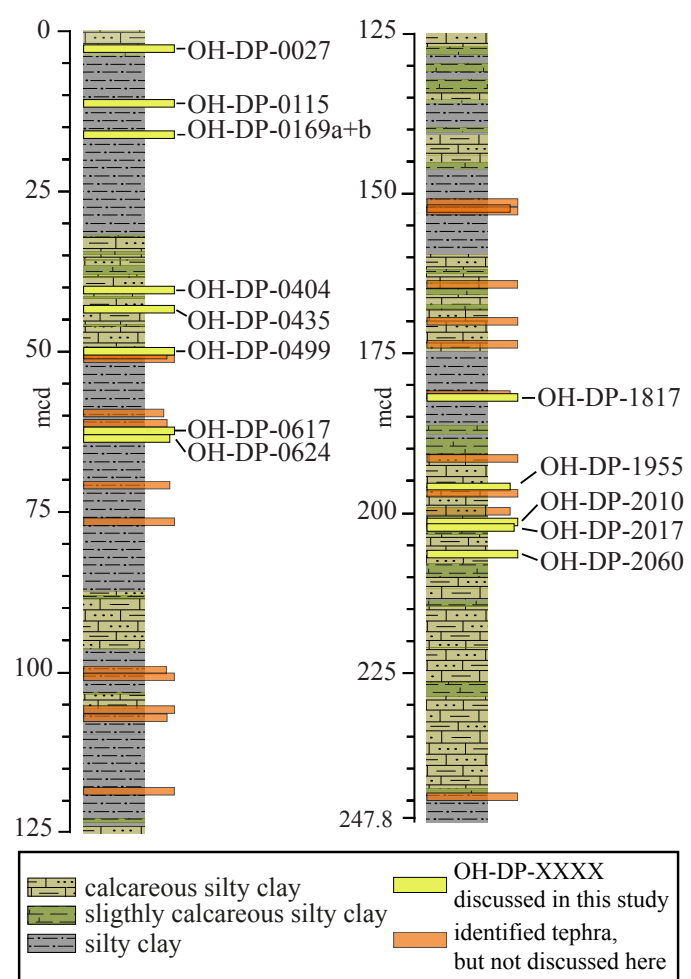
Measured mean	75.84	0.23	11.16	2.23	0.16	0.05	0.09	4.57	4.51	0.03	0.25	0.18	0.03	99.32		Total
Recommended	76.00	0.19	11.50	2.02	0.16	0.08	0.10	4.75	4.47	-	-	-	-	0.03	99.30	

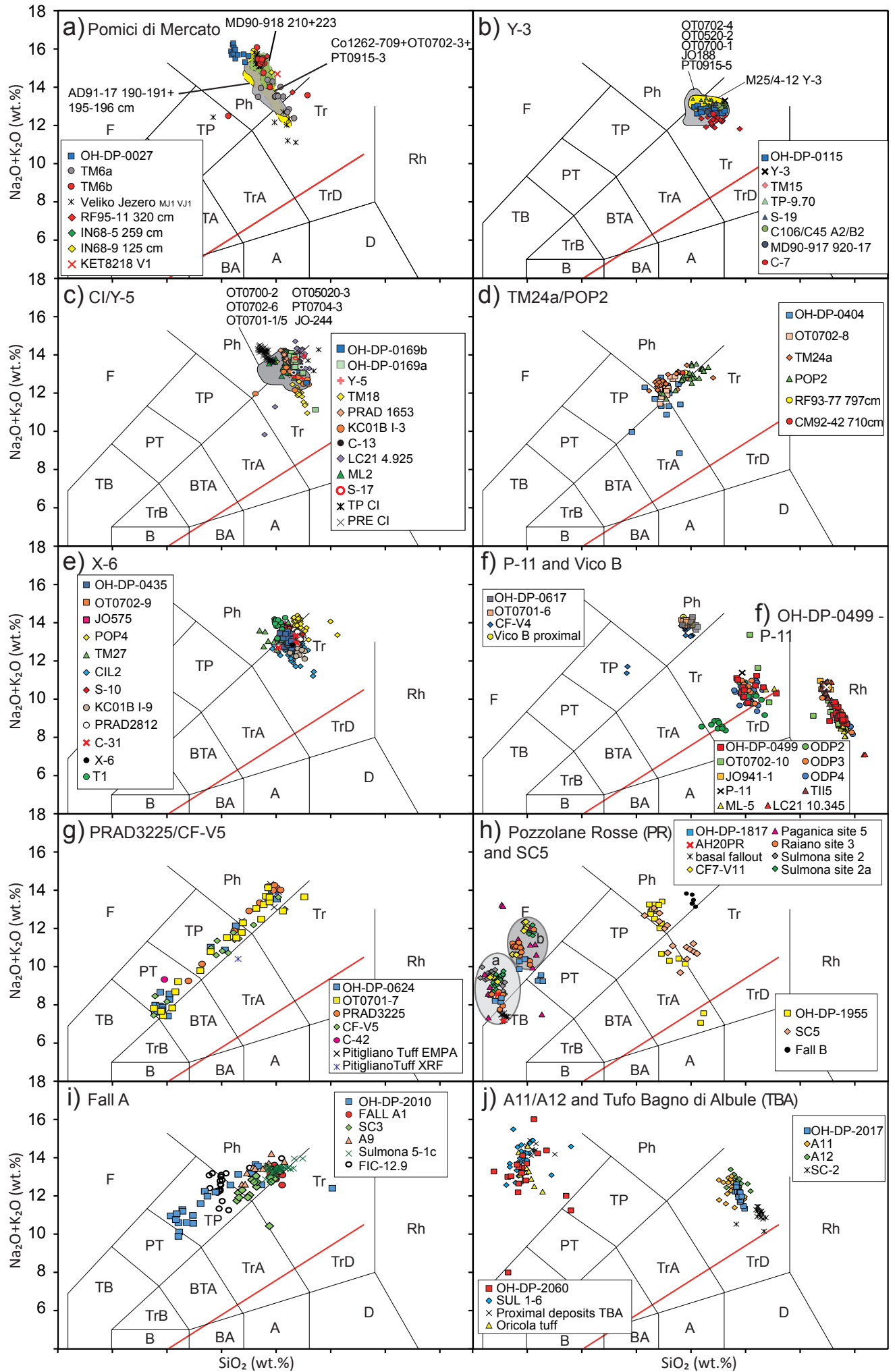
##### Standard 2 - Kakanui Augite

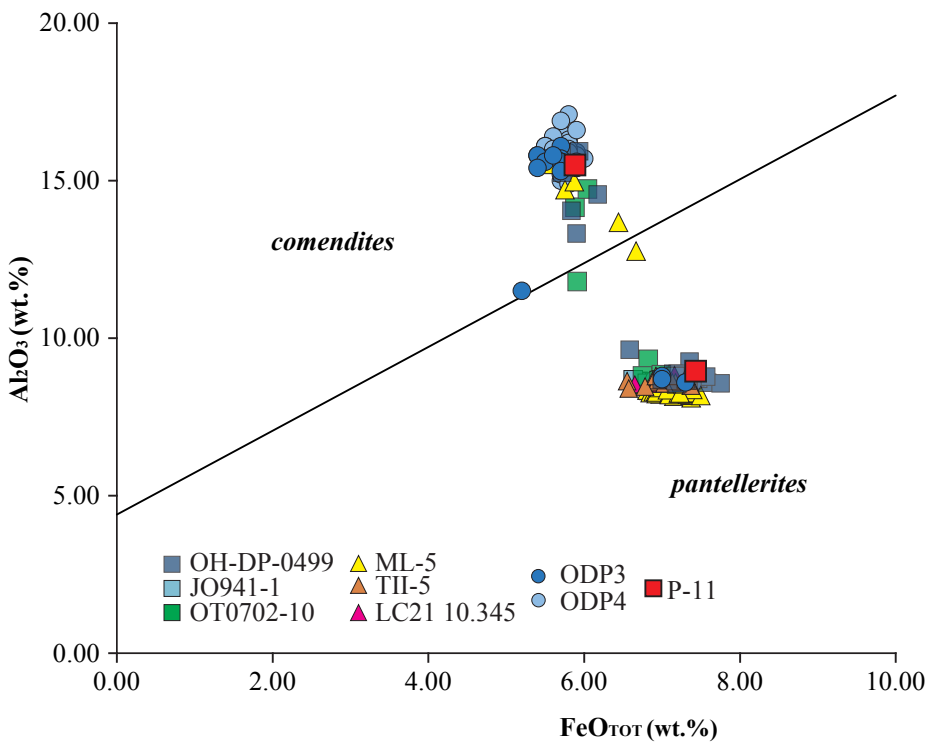
Measured mean	50.79	0.87	8.36	0.09	6.53	16.27	15.95	1.29	-	-	-	-	-	-	100.14
Recommended	50.46	0.84	8.28	0.13	6.51	16.28	16.00	1.30	-	-	-	-	-	-	99.80

Tephra DEEP site	Depth (mcd)	Eruption/ Tephra	Age (ka)	References	recalculated $^{40}\text{Ar}/^{39}\text{Ar}$ ages
OH-DP-0027	2.773	Mercato	8.43–8.63	Zanchetta et al., 2011	N.A.
OH-DP-0115	11.507	Y-3	28.68–29.42	Albert et al., 2015	N.A.
OH-DP-0169	16.933	Campanian Ignimbrite/Y-5	39.28±0.1	De Vivo et al., 2001	39.6±0.1
OH-DP-0404	40.486	POP2	102±2.4	Regattieri et al., 2015	N.A.
OH-DP-0435	43.513	X-6	109±2	Iori et al., 2014	109±2
OH-DP-0499	49.947	P-11	133.5±2	Satow et al., 2015	N.A.
OH-DP-0617	61.726	Vico "Ignimbrite B"	157±3	Laurenzi and Villa, 1987	162±6
<b>OH-DP-0624</b>	<b>62.413</b>	<b>Pitigliano Tuff</b>	<b>158±22</b>	<b>Turbeville, 1992a</b>	<b>163±22</b>
OH-DP-1817	181.769	Pozzolane Rosse	457±4	Karner et al., 2001	457±4
			457±2	Giaccio et al., 2013	457±2
OH-DP-1955	195.566	SC5	493.1±10.9	Giaccio et al., 2014	493.1±10.9
<b>OH-DP-2010</b>	<b>201.049</b>	<b>Sabatini Fall A</b>	<b>499±3</b>	<b>Marra et al., 2014</b>	<b>496±3</b>
OH-DP-2017	201.782	Acerno A11-12	514±6	Petrosino et al., 2014	511±6
OH-DP-2060	206.080	Tufo di Bagni Albule	527±2	Marra et al., 2009	527±2



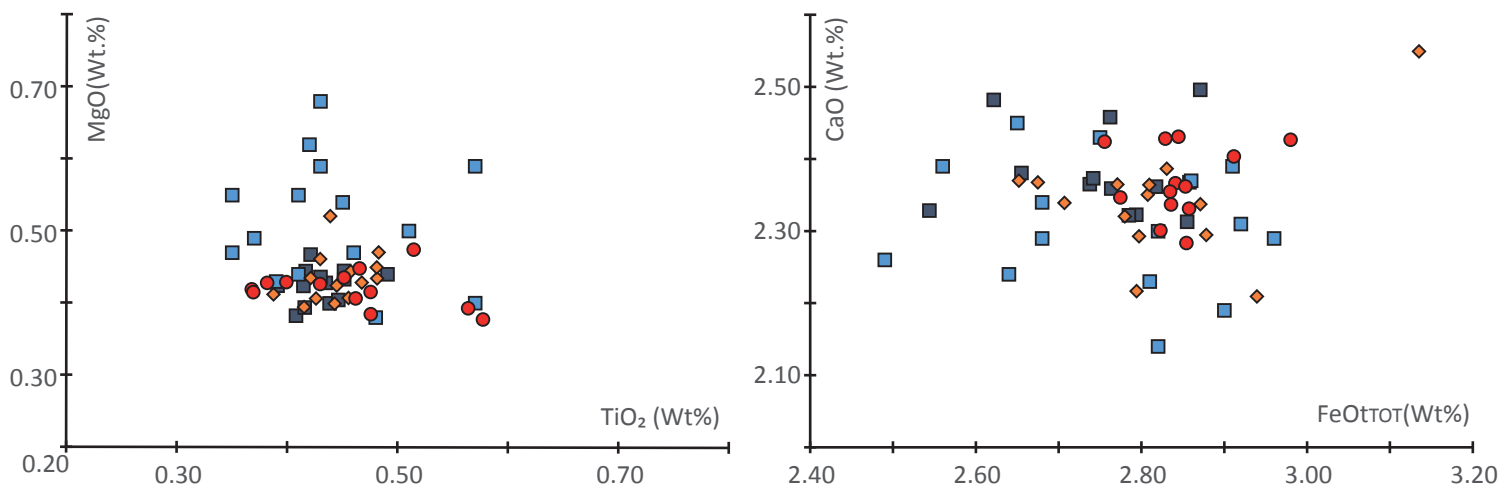




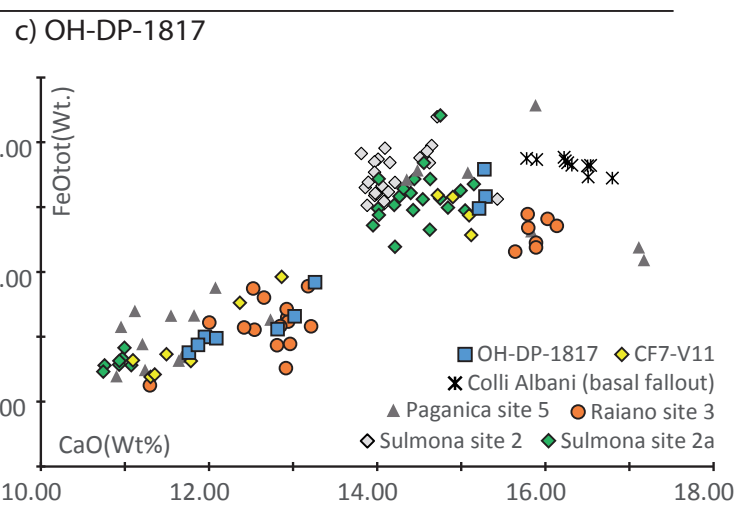
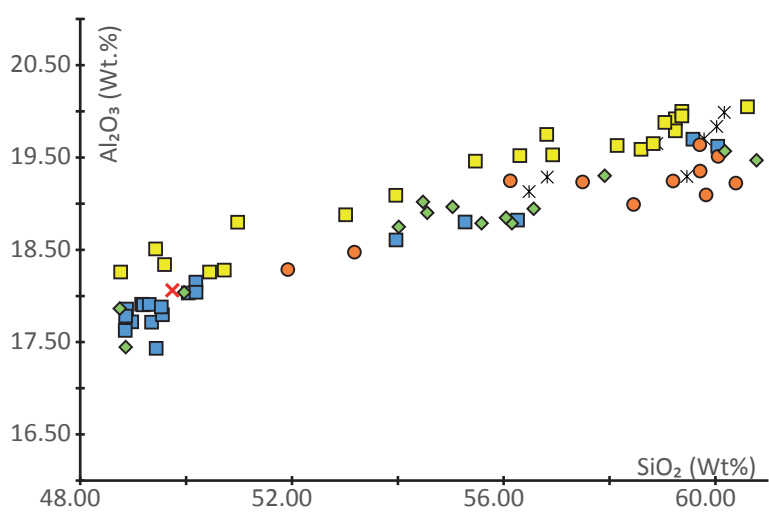
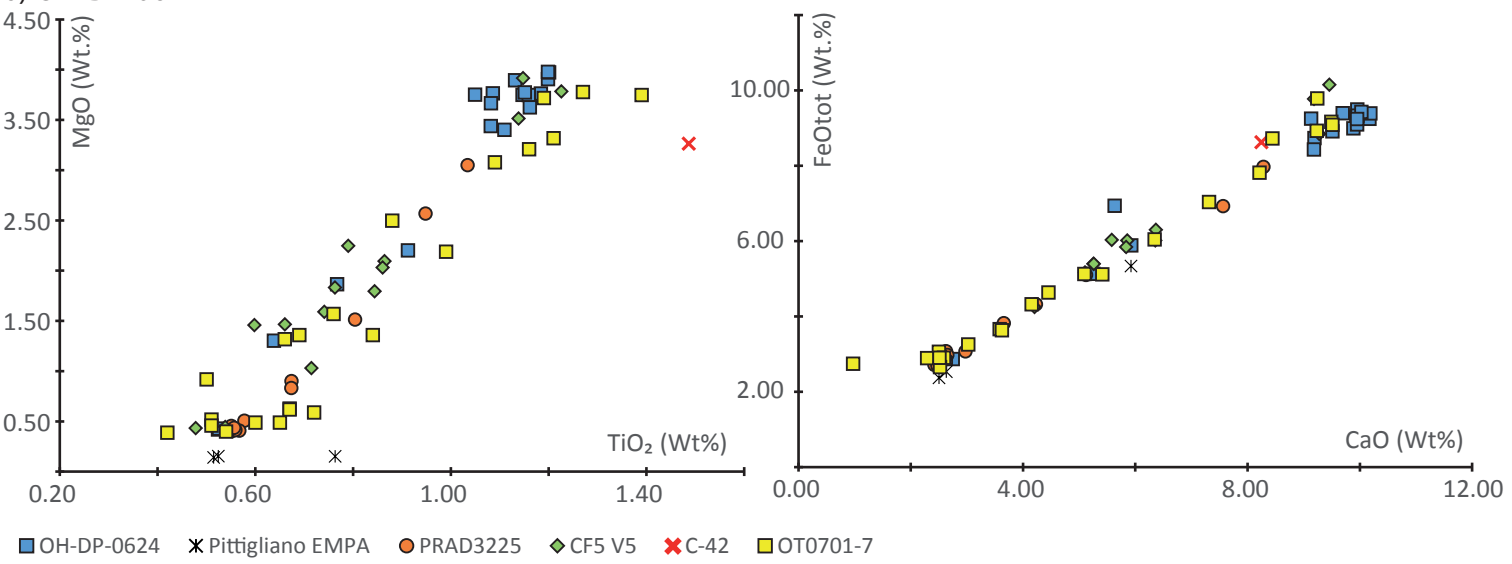


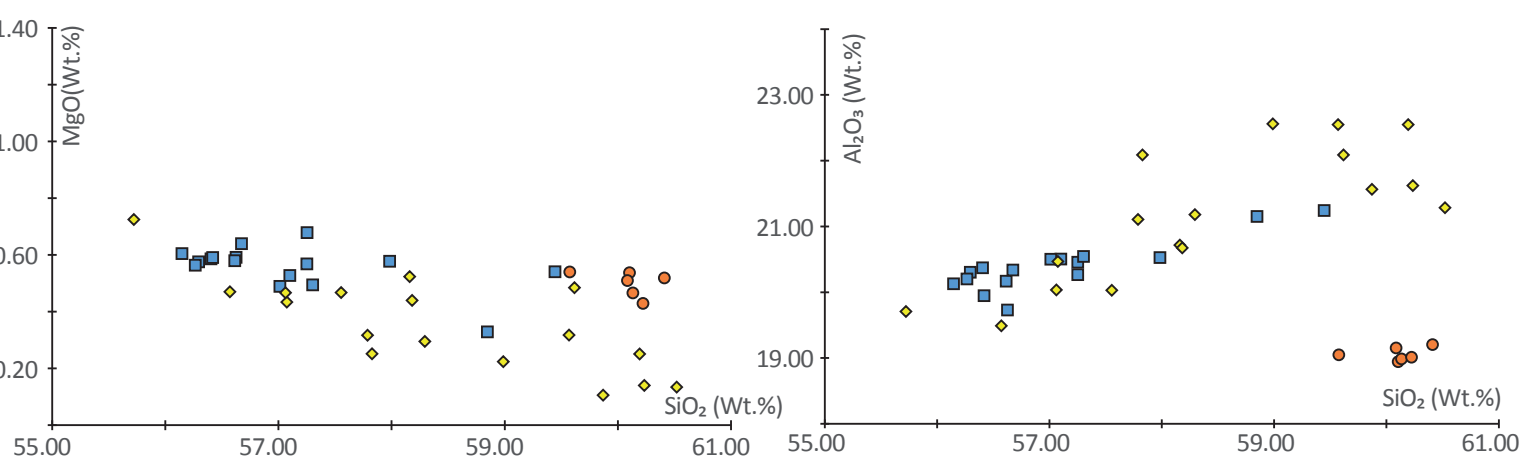
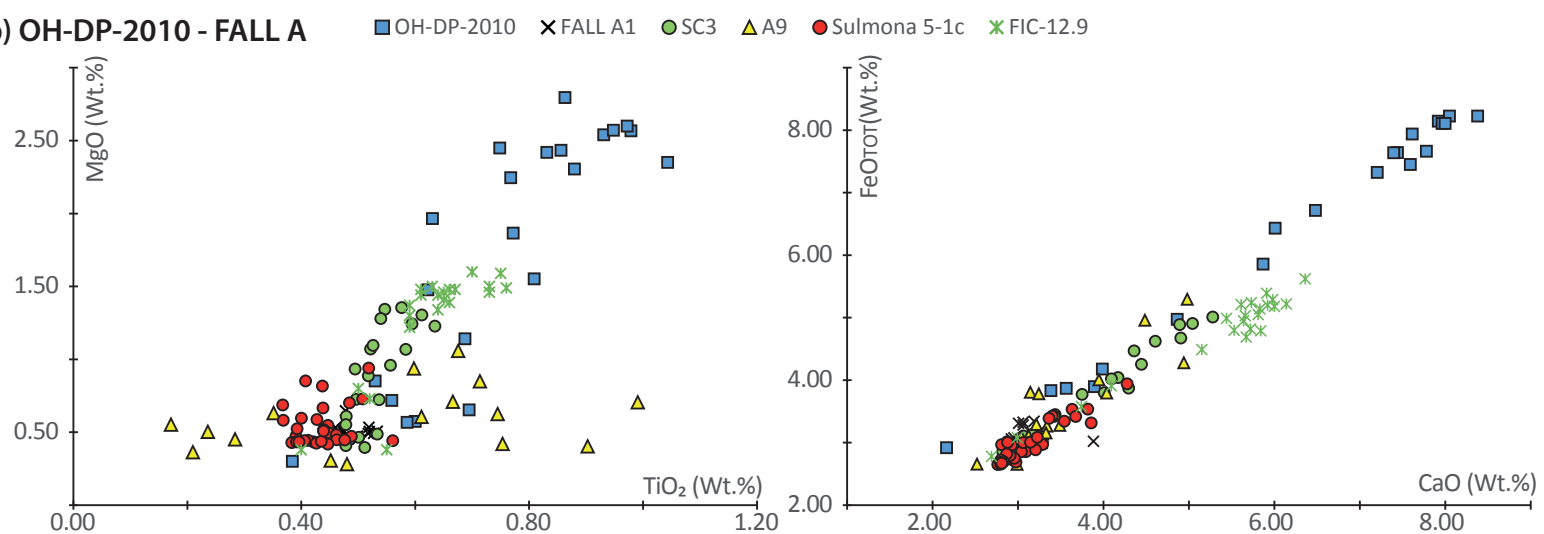
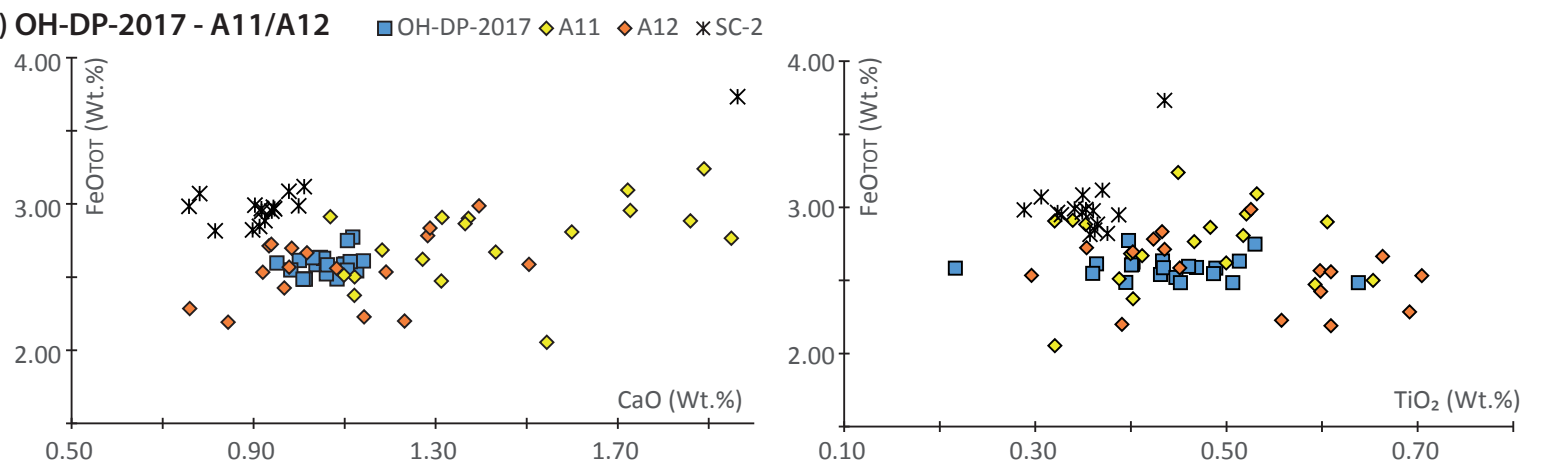
a) OH-DP-0617

■ OH-DP-0617 ■ OT0701-6 ■ CF5 V4 ■ Vico B



b) OH-DP-0624



**a) OH-DP-1955 -SC5** ■ OH-DP-1955 ♦ SC5 ● Fall B**b) OH-DP-2010 - FALL A****c) OH-DP-2017 - A11/A12****d) OH-DP-2060 - Tufo di Bagno Albule**